Fault Detection Method for Inverter Interfaced Distributed Generator Based Microgrid

A PROJECT REPORT

Submitted in Partial fulfillment of the requirements for the award of the degree of

BACHELOR OF TECHNOLOGY
IN
ELECTRICAL AND ELECTRONICS ENGINEERING

by

P. S. D. S. Prasad 520217

G. S. S. N. S. Manikanta 520129

O. Jayasimha Reddy 520210

Supervisor:

Dr. Yadala Pavankumar

Department of Electrical Engineering

National Institute of Technology, Andhra Pradesh

Tadepalligudem, Andhra Pradesh - 534101

May - 2024

APPROVAL SHEET

This Project Work entitled Fault Detection Method for Inverter Interfaced Distributed Generator Based Microgrid by P. S. D. S. Prasad (520217), G. S. S. N. S. Manikanta (520129), O. Jayasimha Reddy (520210) is approved for the degree of Bachelor of Technology in Electrical and Electronics Engineering.

Supervisor

_____

Dr. Yadala Pavankumar

Adhoc Faculty

Dept. of Electrical Engineering

NIT Andhra Pradesh

Head of Department

_____

Dr. T. Ramesh

Assistant Professor

Dept. of Electrical Engineering

NIT Andhra Pradesh

Date:_____

Place:_____

DECLARATION

I declare that this written submission represents my ideas in my own words and where others' ideas or words have been included, I have adequately cited and referenced the original sources. I also declare that I have adhered to all principles of academic honesty and integrity and have not misrepresented or fabricated or falsified any idea/data/fact/source in my submission. I understand that any violation of the above will be cause for disciplinary action by the Institute and can also evoke penal action from the sources which have thus not been properly cited or from whom proper permission has not been taken when needed.

P. S. D. S. Prasad 520217 Date: 01/05/2024	G. S. S. N. S. Manikanta 520129 Date: 01/05/2024	O. Jayasimha Reddy 520210 Date: 01/05/2024

CERTIFICATE

This is to certify that the dissertation work entitled “Fault Detection Method for Inverter Interfaced Distributed Generator Based Microgrid” is a bonafide record of work carried out by “Mr. P. S. D. S. Prasad (520217), Mr. G. S. S. N. S. Manikanta (520129) and Mr. O. Jayasimha Reddy (520210)”, submitted to the faculty of “Department of Electrical Engineering”, in partial fulfilment of the requirements for the award of the degree of Bachelor of Technology in “Electrical and Electronics Engineering” at National Institute of Technology, Andhra Pradesh during the academic year 2020 – 2024.

Mr. P. S. D. S. Prasad, **Mr. G. S. S. N. S. Manikanta** and **Mr. O. Jayasimha Reddy** has worked under my guidance and supervision and has fulfilled the requirements for the submission of this thesis, which to my knowledge has reached the requisite standard. The results obtained here in have not been submitted to any other University or Institute for the award of any degree.

Name of the Supervisor: **Dr. Yadala Pavankumar**
Adhoc Faculty
Dept. of Electrical Engineering
NIT Andhra Pradesh

Name of the HOD: **Dr. T. Ramesh**
Head of the Department
Dept. of Electrical Engineering
NIT Andhra Pradesh

ACKNOWLEDGEMENT

We would like to express a special thank of gratitude to our project guide **Dr. Yadala Pavankumar** (Adhoc Faculty) for his constant support, perseverance guidance thus helping us pivot in the right direction. It was because of his suggestions & continuous efforts that we were able to refine the topic to its core dependable interests & work toward a relevant approach for fault detection method for inverter interfaced distributed generator based microgrid.

We respect and thank **Prof. B. Srinivasa Murthy**, Director NIT Andhra Pradesh for providing us an opportunity to do the project work in the college and giving us all the support and guidance.

We are highly thankful to **Dr. T. Ramesh**. Head of the Department, Department of Electrical Engineering for the guidance and constant supervision as well as for providing necessary information regarding the project and for the constant support in completing the project.

We are also thankful to our faculties who have played a major role in imparting us the knowledge to understand the details of electrical engineering equipped us with the relevant skills to understand industry research scale applications. We would like to thank our beloved families for their kind co-operation and encouragement.

We would like to thank the CRTDH project managers of National Institute of Technology Andhra Pradesh for providing OPAL-RT facilities.

ABSTRACT

A microgrid is a small power distribution system consisting of a cluster of low-power generation units (micro energy sources) capable of operating independently, loads, energy storage, and energy conversion devices with associated protection and control units. Unlike traditional microgrids, the micro sources in all microgrids are inverter-interfaced distributed generators (IIDGs), in which the fault currents are 1.2 - 2 times the rated current. To ensure the stable operation of the microgrid requires to detect the faults within the minimum possible time. The data collected from Waveform Measurement Units (WMUs) are widely used to detect disturbances. When an event occurs, WMUs provide GPS-synchronized measurements of voltage and current waveforms in the time domain captured during the event. Given such data, a Lissajous curve can be developed, which is a graph constructed by plotting one waveform versus another. By utilizing this phenomenon, a new algorithm has been developed to detect and locate faults within the microgrid.

Keywords: Distributed Generation, Fault detection, Low voltage ride through, Microgrid.

TABLE OF CONTENTS

LIST OF FIGURES

LIST OF TABLES

LIST OF ABBREVIATIONS

CB	Circuit Breaker
CERTS	Consortium for Electric Reliability Technology Solutions
DER	Distributed Generation Resource
DG	Distributed Generator
DPMU	Distribution-Level Phasor Measurement Unit
ESS	Energy Storage Systems
FRT	Fault Ride Through
GCP	Grid Connection Point
HIF	High Impedance Fault
HIL	Hardware- in-the-Loop
IDMT	Inverse Definite Minimum Time
IEC	International Electrotechnical Commission
IIDG	Inverter Interfaced Distributed Generator
WMU	Waveform Measurement Unit
LIF	Low Impedance Fault
LG	Line to Ground
LL	Line to Line
LLG	Line to Line Ground
LLL	Line to Line to Line
LLLG	Line to Line to Line Ground
LVRT	Low Voltage Ride Through
MCC	Microgrid central controller
PCC	Point of Common Coupling
PLL	Phase-Locked Loop
PMU	Phasor Measurement Unit
PPG	Photovoltaic Power Generation
PSO	Particle Swarm Optimization
RTDS	Real Time Digital Simulator
SI	Similarity Index

TG	Turbine Generation
UVRT	Under Voltage Ride Through
VUF	Voltage Unbalance Factor

CHAPTER – I

INTRODUCTION

1.1 OVERVIEW

A microgrid consists of different electrical loads, energy storage systems (ESS), and distributed generators (DGs). There are two ways that microgrids can function, the first one is grid connected mode in which the microgrid will be integrated to the utility grid and islanded mode of operation where it will work independently [1]. Most of the micro sources in the microgrid are inverter-interfaced distributed generators (IIDGs), and the fault characteristics of IIDGs differ from those of conventional synchronous generators. The maximum output fault current of the IIDG is typically limited to 1.2-2 times the rated current [2]. Traditional methods like overcurrent protection and distance-based relays are inadequate due to the bidirectional power flow and renewable-based distributed generators (DGs) present in microgrids. Using IIDG-based microgrids, these characteristics create significant challenges for fault detection. It is necessary to discover an appropriate fault detection technique for microgrids in order to support the practical implementation of these systems. In the past few years, researchers have studied microgrid fault detection techniques extensively.

In recent years the utilization of waveform measurement units (WMUs) as a smart sensor has been introduced. The WMU can provide precise information of the time synchronized current and voltage waveform measurements and has high reporting rate. These WMUs can be utilized to observe the voltage and current waveform under disturbances such as faults, capacitor switching's, islanding of the loads and DGs etc., which has to be identified in less time for safe and continuous operation of the microgrid. The voltage and current waveforms can be used to generate the Lissajous figure [3,4].

1) It is observed that the Lissajous curve shape changes under different conditions. During normal conditions, the Lissajous curve is elliptic; however, when a fault arises, its shape changes. Therefore, on the basis of this phenomenon a novel method for microgrid fault detection is developed.

2) The change in the Lissajous curve results the change in the area of the curve. Hence two successive areas are monitored to develop the fault index in the proposed approach. Once a fault occurs, the area changes, indicating that fault has occurred and the similarity index values can identify the start time of fault event.

3) The proposed algorithm has considered the thresholds to distinguish between the faulty phase and healthy phase of the feeders.

This study offers a novel technique to detect low impedance fault in the microgrid by using the Lissajous figure patterns. Additionally, the HIL testing analysis demonstrates the high accuracy of the suggested method for practical applications. However, the proposed method has not considered the high impedance faults, which will be analyzed in the future works.

1.2 LITERATURE SURVEY

A microgrid is a small power distribution system, which consists of distributed generations (DGs), energy storage devices, energy conversion devices, loads, corresponding supervision and protection equipment's [5]. It will play an important role in the future of smart grid construction [6]. Unlike traditional distribution networks, the majority of micro-sources in a microgrid are inverter interfaced distributed generators (IIDGs), and the fault features of IIDGs are different from those of synchronous generators. The maximum output fault current of the IIDGs is generally limited to 1.2~2 times that of the rated current [2]. Meanwhile, parts of IIDGs have the disadvantages of intermittence and randomicity, and a microgrid can be operated in grid-connected mode or islanded mode, which lead to a large difference in the fault current level with the change in the microgrid operation mode. Likewise, the dispersion of the installation of DGs leads to bidirectional fault currents in a microgrid and DGs cause changes to fault current inside the microgrid, several issues affect the overcurrent protection initially designed for the radial network. Blinding of protection, false tripping, overreach of relay and mis coordination between protection devices are several important effects that result from fault current changes in the network and DGs partial contribution to a fault [7-13]. The previously mentioned impact on protective devices is due to the contribution of the DG to fault currents that were not included in the initial design and fault calculations of the system [14]. These factors present new fault detection issues with the microgrids consisting of

IIDGs. To promote the practical application of microgrids, it is a necessary and urgent task to find a suitable fault detection method for microgrids [15]. In recent years, scholars have performed much research on the fault detection methods of microgrids. Reference [16] proposed a traveling wave-based protection scheme for microgrids. The mathematical morphology technology was utilized to calculate the current traveling waves. Fault detection was completed by comparing the time of the initial traveling wave to the related protection devices. However, since the feeders in a microgrid are generally short, it is difficult to extract and distinguish transient traveling wave signals after multiple reflections and refraction have occurred. Meanwhile, the traveling wave signals are easily impeded by the non-fault event interference. An impedance-based fault detection scheme was proposed in [17]. The positive-sequence component using phasor measurement units and the designed microprocessor-based relays, along with a digital communication system, were used to detect the fault location. The proposed scheme had the ability to protect radial and looped microgrids against different types of faults. However, the measuring precision may be disturbed by the harmonics and transient process, and its performance is easily affected by the short-circuit transition resistance, thus making it unsuitable for the short line conditions of the microgrid. A differential sequence component protection scheme for microgrids with inverter-based distributed generators was proposed in [18]. The protective devices were implemented as distributed statistical classifiers, and a data mining approach was used to identify the relay settings and parameters. The symmetrical components of the current were selected as the fault characteristics. When HIFs occur, the symmetrical components of the fault currents are not sufficiently larger than the nominal load currents, and the protection's sensitivity is low. Additionally, the scheme can only locate faults in the transmission line. An adaptive protection scheme was presented in [19]. The scheme could solve problems arising from both grid-connected and islanded operation modes. An automatic readjustment of relay settings is triggered when the microgrid changes from the grid-connected mode to the islanded mode. However, for fault detection during adaptive protection, all possible configurations of the microgrid need to be considered beforehand, which is difficult to achieve. Similarly, the calculation of the short-circuit fault current is difficult for a microgrid with different operating modes; thus, the current-setting value of the adaptive fault detection is difficult to select. Additionally, the size of the neutral-point

grounding impedance has a great effect on the fault characteristic of microgrids. Particularly, when a high-resistance fault occurs, the fault current or voltage variation is very small, so the setting value is difficult to determine [20]. To solve the fault detection problem of high-impedance faults (HIFs) in microgrids, a novel method for modelling HIFs was demonstrated to show how the fault detection scheme can protect against them [21]. The relays can detect the faults by sampling the current waveform at 16 samples per cycle or more. However, the differential fault detection scheme requires a precise synchronous clock and cannot eliminate the influence on differential currents caused by the capacitive current, and the disconnection of DGs may cause some problems [22]. Fault components are caused by a fault itself, independent of the load component, especially a positive-sequence fault component, which always exists in all types of faults [23]. Thus, some researchers have put forward the fault detection method of a microgrid based on the fault components principle. A fault direction scheme for a radial distribution system using the phase change in a sequence current was presented in [24]. The pre-fault current phasors were used for fault detection, fault classification, and other applications. However, the scheme can only be applied to metallic short-circuit faults, and the fault in branch feeders cannot be detected. Reference [25] proposed a fault detection method using the phase change in the negative-sequence current. A directional relaying algorithm during single-pole tripping using the phase change in the negative-sequence current was proposed. However, the algorithm cannot identify the faulty phase and does not refer to a fault in the branch feeder. A voltage-independent fault detection method was presented in [26]. It uses the phase information of the current fault components from at least three feeders connecting to the bus bar to identify the fault direction. In [27], an integrated wide-area protection scheme based on the fault components principle was proposed. A fault location was realized by comparing the phase difference of the positive-sequence current fault components to the main feeder and slave feeders in different area protection units. Moreover, for the above fault components principle, the traditional fault components additional network analysis method was used.

Meanwhile, the specific control strategy of IIDGs has not been considered, and thus, the IIDGs are a simple equivalent to a constant power or current source. The fault control strategy and the equivalent fault model of IIDGs are presented in [28], [29], but the relevant

fault detection method of microgrids is not involved. Based on the LVRT requirement of direct grid-connected DGs [30], [31]. In [32], proposes a fault detection method for microgrids with grid-connected PQ-DGs. The influence of a PQ-DG's control strategy on the fault characteristics in the operating conditions of HIFs and LIFs are analyzed. Based on the phase differences between the positive-sequence fault components of the bus voltage and the positive-sequence fault components of the currents in the feeders, a new fault detection method and its fault criteria are proposed.

The deployment of smart meters over the past decade has provided a wide range of benefits for data-driven monitoring and situational awareness in power distribution systems [33]. However, there are major limitations to smart meters; such as due to their slow reporting rates; at once every 15 minutes. The reading interval, resolution, and time-precision of measurements have drastically improved in recent years by the use of distribution-level phasor measurement units (DPMUs). D-PMUs provide GPS-synchronized voltage phasor and current phasor measurements in power distribution circuits [34], [35]. Applications of D-PMUs are discussed in several paper, e.g., in [36], [37]. However, PMUs are not suitable to study power quality events in distribution systems. Examples of such events are incipient faults and high impedance faults. Motivated by the above facts, a new class of smart grid sensors has been introduced recently, called waveform measurement units (WMUs).

WMUs are a new class of smart grid sensors that provide precise time-synchronized voltage and current waveform measurements in time domain [38] – [46]. A typical WMU has a reporting rate of 256 to 512 samples per cycle; and a time accuracy of 1 μ sec. Therefore, the wave form measurements from multiple WMUs are synchronized precisely; making them appropriate for the analysis of various disturbances in power distribution networks [47]. However, data availability in itself does not lead to enhanced grid intelligence. We need to translate the WMU data to insightful information.

Lissajous figure can be developed utilizing the voltage and current waveforms [48]. The Lissajous figure reveals different behavior under different conditions which can be utilized to identify the cause of events in the system. In general, a Lissajous curve is a graph that is constructed by plotting one waveform versus another waveform Different types of Lissajous curves are traditionally used in signal and image processing; such as to analyze

electrocardiogram and dielectric discharge [49]. Lissajous curves have occasional applications also in power engineering; such as to diagnose internal faults and winding deformations in power transformers [50]. Therefore, the authors in this work seek to propose a new fault detection method for microgrid by utilizing the characteristics of the Lissajous figure.

1.3 PROBLEM STATEMENT

In traditional microgrids, which utilize inverter-interfaced distributed generators (IIDGs), fault currents typically range from 1.2 to 2 times the rated current of the IIDGs and the power direction becomes bidirectional. Detecting faults in microgrids quickly is crucial to ensure their stable operation. However, in conventional power distribution systems, fault currents can be as high as 10 times the rated current, making fault detection relatively straightforward using protective devices.

The problem arises when fault detection in microgrids becomes challenging due to the lower fault current levels compared to conventional power distribution systems and bidirectional power flow. This difficulty in fault detection necessitates the development and implementation of more advanced techniques to ensure the reliability and stability of microgrids.

1.4 OBJECTIVES

- Implementation of low voltage ride through (LVRT) in the IIDG'S.
- Identifying the patterns of Lissajous figure.
- Developing the suitable index for fault detection.
- Selecting the threshold.
- To implement the proposed approach in real time digital simulator (OPAL-RT).

1.5 THESIS ORGANIZATION

The contents of this thesis have been divided into the following chapters

Chapter II: Microgrid

This chapter introduces the microgrid system, microgrid supervisory control, distributed energy resources and fault detection issues in network with DGs.

Chapter III: Control Strategy of IIDGs

This chapter presents the control scheme for DGs, low voltage ride through (LVRT) and proposed microgrid test system.

Chapter IV: Proposed Fault Detection Technique

This chapter deals with different type of Lissajous patterns, developing the suitable index and proposed fault detection method.

Chapter V: Simulation Results

This chapter presents comprehensive performance analysis of LVRT and different type of faults.

Chapter VI: Conclusion and Future Scope

This chapter tells about the conclusion and future scope.

Appendix: Best Paper Award and Conference paper

CHAPTER – II

MICROGRID

2.1 MICROGRID SYSTEM

Microgrid is a combination of Distributed generation resources (DER), Energy Storage Systems (ESS) and various types of electrical loads. Microgrid appears as a single component with respect to the main grid which is governed by control signals. The DERs in the Microgrid may be micro turbines, fuel cells, solar cells, wind turbine, or any conventional or non-conventional power sources. Microgrid can be defined as a collection of Loads, DER and ESS operated in synchronization for supplying reliable electric power, which is linked with the host power system at the consumption level to a single point of connection, known as the Point of Common Coupling (PCC) [51][52]. It is generally at low voltage side of distribution power system. Microgrids are known as building blocks of smart grids. The objective of the microgrids is to deliver electricity in sustainable, economical and secure way by intelligent monitoring, control and self-healing technologies. To the utility microgrid can be a sort of load which can call for power at any time e.g. at night as in case of a solar cell which does not have power at night or at cloudy day [53]. Microgrids seems like a new, local and small-scale grid which maximizes its local resources available in a geographical region and minimizes the AT&C losses. The microgrids operate in two types, i.e. island mode and grid connected mode.

2.1.1 Island Mode

Microgrid, which do not have PCC are termed as isolated microgrid or it can simply be termed as standalone microgrid. The remote areas, which are not connected to the utility grid due to the technical or financial restrictions are examples of this type of grid and power can be supplied to these areas through standalone microgrid. The islanding capability lowers the outages and improves service, power quality and reliability. Islanding can be either planned or unplanned. Planned islanding can occur in states such as planned maintenance or when power quality of the utility main grid can threaten microgrid

operation and quality. Unplanned islanding can happen due to faults and other spontaneous proceedings that are indefinite to the microgrid.

2.1.2 Grid Connected Mode

In this mode, the microgrid is connected with electricity grid. It can also be of two types i.e. one, which is connected with grid but does not supply surplus power to the grid and the other which supply surplus power to the utility grid. Frequency should be synchronized with the main electric grid so that electricity can be transfer to the main grid without any technical issues. There are various techniques for matching the different parameters of the microgrid like artificial intelligence techniques such as fuzzy logic, neural network, genetic algorithm, Particle Swarm Optimization (PSO) etc. The work of the PCC is to isolate and link the main and micro grid. In case of peak demand when DER are not able to fulfil the demand then it is fulfilling by the main grid through PCC. This mode ensures the non-stop supply of power as if there is fault in the DER, the utility grid can act as a backup power source. Hence load shaving is minimum in this case [54].

2.2 MICROGRID SUPERVISORY CONTROL

In support of maximum output power from the microgrid system two supervisory control strategies are discussed in various literature [55][56], which are Centralized and Decentralized.

2.2.1 Centralized Control System

In this system, there is an microgrid central controller who takes all the decisions. Microgrid central controller (MCC) gathers all information regarding forecasted generation and load demand, SOC of each storage devices, utility grid status and after that perform multi-stage optimization as per the constraints related to power flow, market and network parameters etc. and then direct each DER for power production. In case of shortage of power, guide for unit commitment too. This system requires heavy computation system as well as reliable and advanced communication system.

2.2.2 Decentralized Control System

When number of DERs are connected then their owner may be different so it creates lots of management issues in centralized control system and a certain level of intelligence

is required so as to manage critical loads of its own grid, which is not possible in it. In decentralized control system, each DER have its own local controller who is responsible for maximum power generation as well as for meeting load demand. The bids for energy selling/purchasing are sent to central microgrid operator. Local controller manages its own grid and adjust the loads as per energy availability. Multiple agents are used for controlling purpose along with artificial intelligence techniques. There are more co-ordinations between the local controllers of the different microgrid as compared to central control system as well as freedom for optimized operation of the microgrid. There is very less requirement of communication system.

2.3 DISTRIBUTED ENERGY RESOURCES

Distributed energy resources/ distributed generation (DG)/ dispersed generation/ embedded generation/ decentralized generation are electric power sources connected to the distribution network [57]. Distributed resources can be set up in distribution system on either the consumer end or utility end of the meter. They can be owned and operated by utility grid or by consumer. There are number of advantages of DER like consumption of power at generating point which minimize the transmission losses as well as provision of power at inaccessible region [58]. The distributed energy resources are dispatchable (which can adjust their output power as per the requirement i.e. hydroelectric, natural gas, pumped storage power plant, biomass, geothermal, ocean thermal etc.) and non-dispatchable (which are not able to adjust their output power as per need i.e. wind, solar, tidal, wave etc.) DERs supplies real as well as reactive power. They can influence real as well as reactive power flow so as to manage demand as well as transmission loss. During fault condition or disturbances, the DER can operate as low voltage ride through (LVRT) or Fault ride through (FRT) or under voltage ride through (UVRT) for some specified time periods in milliseconds and voltage range as per norms of utility. In this condition, they remain connected to the grid and temporarily supply the reactive power for specified time period [59]. Out of these different distributed energy resources the special attention within this section is given on photovoltaic and wind power generations.

2.3.1 Photovoltaic Generation

A PV system is an interface that converts light into electricity. A photovoltaic cell is the fundamental generating unit of a PV system, which in itself generates miniscule power. These are connected in either series or parallel to produce higher voltage or current levels. PV modules are the basic building blocks of a PV system. A Photovoltaic panel includes one or more PV modules that are wired together as a field installable unit. A PV module power output depends upon different factors that include temperature, incident irradiance, material, etc. Mathematically, the power output of a PV module can be expressed as [60]:

$$P_{PV} = P_{STC} \frac{G(\beta,\alpha)}{G_{STC}} [1 + \gamma(T_C - T_{STC}) \qquad (2.1)$$

Where is the output Power of PV module under standard test conditions (STC), $G(\beta,\alpha)$ incident irradiance falling on the solar panels, G_{STC} incident irradiance under STC, γ power temperature coefficient, T_{STC} temperature in $°C$ under STC and T_C cell temperature. For equation (2.1) the cell temperature T_C plays very important role which can be expressed as,

$$T_C = (T_a - 273) + \frac{G(\beta,\alpha)}{800} (T_N - 20) \qquad (2.2)$$

Here, and are the ambient and nominal operating cell temperature.

2.3.2 Wind Turbine Generation

The principle of operation of wind turbines is very simple. The wind energy rotates the blades around a rotor which is connected to the generator through main shaft. Wind turbines are fixed at a height with the help of a tower. Mathematically, the wind turbine power can be given as [60],

$$P_{WT} = \frac{1}{2} \rho A C_P V_Z^3 \qquad (2.3)$$

Where P_{WT} is the output power of the wind turbine, ρ the air density $(in\ kg/m^3)$, V_Z wind speed at hub height $(in\ m/s)$, A rotor swept area $(in\ m^2)$, C_P power coefficient of wind turbine. The values of rotor swept area A and wind turbine power coefficient C_P are provided by the wind turbine manufacturer itself. Air density is affected by the environmental conditions such as temperature, atmospheric pressure, etc. For equation (2.3) the air density ρ plays very important role that can be given as,

$$\rho = \frac{M.p}{R.T_a} \qquad (2.4)$$

The term M represents the molar mass of air $(in\ kg/mol)$, p atmospheric pressure $(in\ N/m^2)$, R universal gas constant $(in\ J/K\ mol)$. The wind turbine power estimation requires the extrapolation of the wind speed at turbine's hub height.

2.4 FAULT DETECTION ISSUES IN NETWORK WITH DGS

The integration of DGs with distribution network can give rise to several fault detection related challenges. Some of them are discussed below.

1) Variation in fault current: Integrating DGs alters fault current behavior due to additional impedances. This can lead to non-linear fault current responses, especially with rotating-based DGs generating higher fault currents than inverter-interfaced DGs (IIDGs). In islanded mode of operation, due to the presence of inverter interfaced DGs inside the microgrid, the fault current contribution from the DGs is limited to about twice the rated current of the power switching device used in the inverter. Consequently, over-current protection devices may not activate with the limited fault current contribution of IIDGs.

- Insufficient fault current contribution from inverter-interfaced DG could not reach overcurrent relay breaking current.

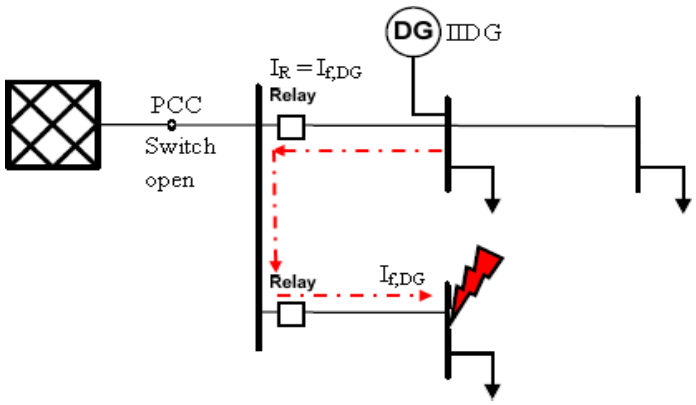

Fig. 2.1 Fault current contribution of utility grid and DG

2) Bi-directional flow: In both grid-connected mode and islanded mode of operation, due to the presence of DGs inside a microgrid, the power and fault current flows bi-

directionally. As a result of this, conventional protection strategies used for radial distribution system do not work properly.

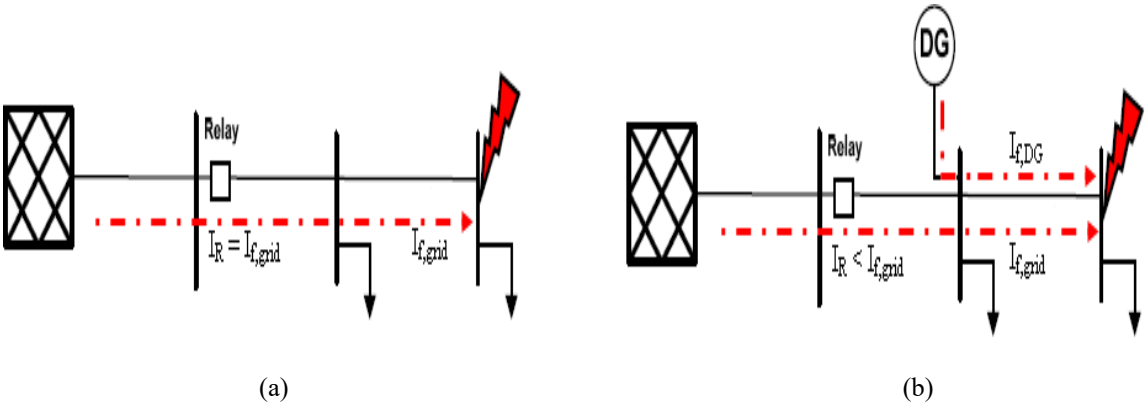

(a) (b)

Fig. 2.2 Bi-directional current flow

- Power and short-circuit current can flow bi-directionally when DG is incorporate in microgrid.

3) Unintentional islanding: These islands are formed when DG continues to energize a location of utility grid even though that location of utility is disconnected from the rest of the system. This can be unsafe for the utility equipment as well as the workers. It also prohibits the automatic reconnection of the isolated part.

4) Sympathetic/False tripping: In grid-connected mode of operation, when a DG is connected to one of its feeder and fault occurs on an adjacent feeder, the current

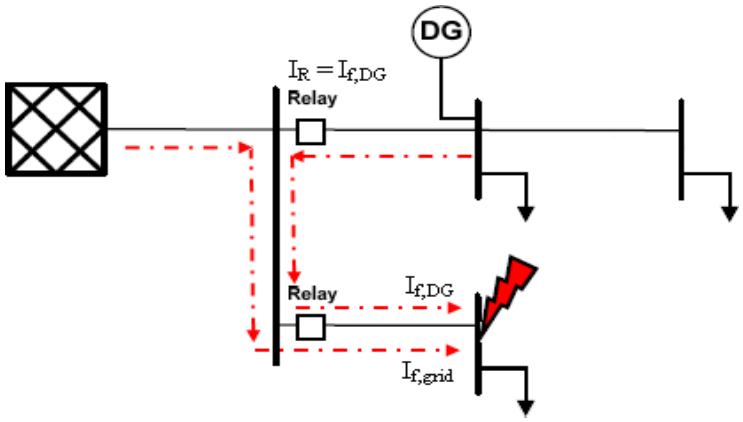

Fig. 2.3 Sympathetic tripping

contribution from the DG (if the DG capacity is sufficiently large) could exceed the feeder overcurrent protection pickup current setting.

- Relay on feeder with DG false trips due to sufficiently large fault current contribution from DG.

This phenomenon can cause tripping of healthy feeder for a fault on a neighboring feeder. When the DG located near to the substation in-feed to a fault and if the value of IIDG becomes appreciably large, then the relay activates and unnecessarily isolates the healthy feeder.

5) overreach: In grid-connected mode of operation, when a fault occurs downstream from DG connection point, total short-circuit current increase due to contribution from DG.

$$I_{f\_total} = I_{f\_grid} + I_{f\_DG}$$

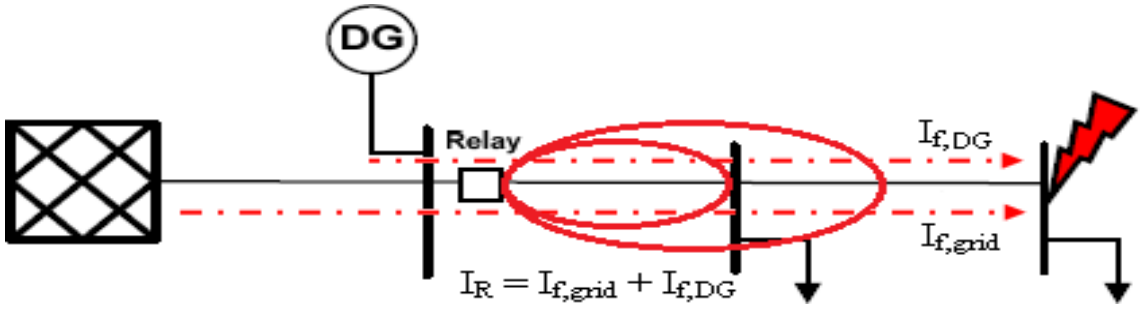

Fig. 2.4 Overreach

- Relay overreach due to increased fault current from DG contribution/Relay delayed trip due to decreased fault current from main grid.

6) underreach: In grid-connected mode of operation, when a fault occurs between the

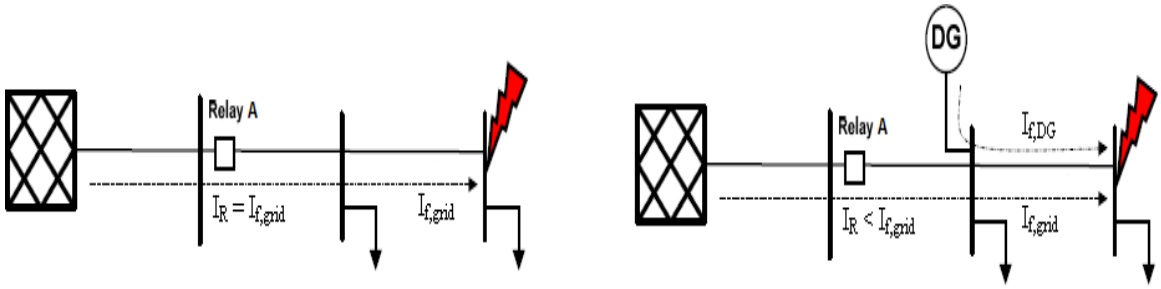

(a) (b)

Fig. 2.5 Underreach

main grid and DG, the current contribution from the main grid is reduced because of partial contribution from the DG.

- Relay A under-reach due to reduction of main grid fault current contribution.

Changes in fault current levels due to DG integration can lead to protection relay underreach (failing to detect faults) or overreach (erroneously tripping for distant faults), affecting system reliability and coordination.

6) Recloser problems: Protection of overhead distribution feeders with automatic reclosers is a very efficient way to protect against temporary disturbances and minimize the number of supply interruptions. because of the coordination between the reclosers and the lateral fuses permanent faults are cleared in a selective way. connection of to these type of feeders causes several protection problems at the same time. First of all the fault current detection by the recloser is affected by the generator contribution and can lead to a detection problem. secondly the coordination between reclosers or fuse and recloser can be lost which directly causes selectivity problems. This is explained in more detail with the feeders shown in Fig. 2.6.

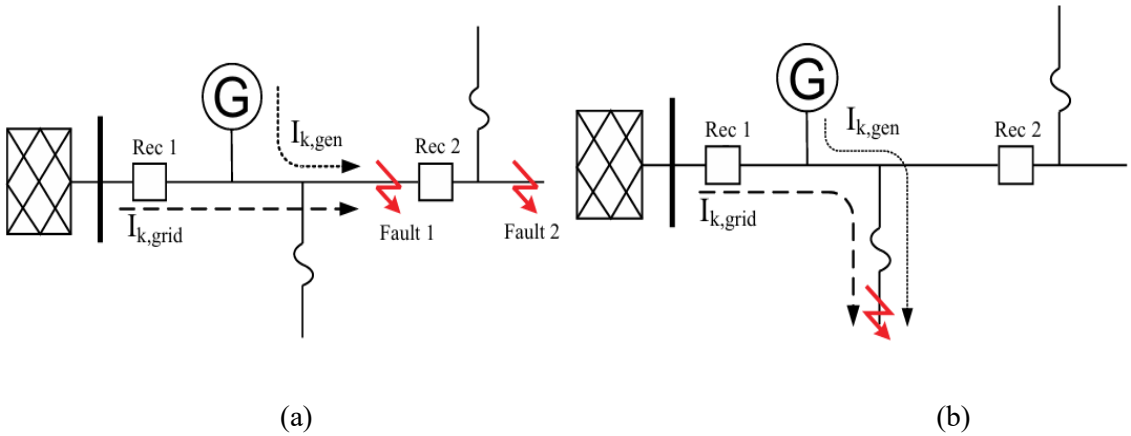

Fig. 2.6 (a) Effect of DG on recloser operation, (b) Recloser-Fuse-DG coordination

In Fig. 2.6 (a), for the Fault 1, the current sensed by the recloser Rec 1 is $I_{k,grid}$ which decreases due to DG contribution, and hence leads to delayed or no detection. For the Fault 2, the current seen by the Rec 2 is greater than Rec 1 because of increase in total fault current in the presence of DG. Therefore, it becomes important to check the maximum

interrupting rating of Rec 2 in case of end-line faults. In Fig. 2.6(b), the reclosers are coordinated with the fuse, and programmed with both a slow and a fast Inverse Definite Minimum Time (IDMT) curve. The DG penetration in distribution networks increases the possibility of a fuse blowing out on a temporary fault before the recloser following fast IDMT curve operates [64].

CHAPTER – III

CONTROL STRATEGY OF IIDGs

3.1 INVERTER INTERFACED DISTRIBUTED GENERATORS (IIDGS):

Unlike traditional distribution networks, the majority of micro-sources in a microgrid are inverter interfaced distributed generators (IIDGs), and the fault features of IIDGs are different from those of synchronous generators. The maximum output fault current of the IIDGs are generally limited to 1.2 ~ 2 times that of the rated current [2]. The unbalanced load present in the distribution network causes voltage unbalance which has many adverse effects. Voltage unbalance factor (VUF) defined by the International Electrotechnical Commission (IEC), can be used to analyze the voltage quality. Due to the adverse effects of voltage unbalance, VUF has a limitation of acceptable compatibility level which varies from country to country and the range is 1 – 5%. As far as power quality is concerned, it is better to consider VUF to be less than 2% to maintain the IEC standards. Majority of the DGs are connected through power electronic interfaces to the microgrid, which are known as inverter interfaced distribution generators (IIDGs). These IIDGs have different control strategies based on the connection type to the micro grid. When unbalanced load is applied to the load bus, the load bus experiences consumption of negative sequence current (I^{-}), which causes voltage unbalance in the microgrid. The DGs in the microgrid can be utilized as compensation units for voltage unbalance compensation.

PQ control strategy is used in grid connected mode of operation, in which the control loop produces d and q reference signals which are responsible for the active and reactive power control of the DG. The voltage and frequency references are obtained from the utility grid and PLL synchronizes the converter operation with the grid. In addition, in grid connected mode, low voltage ride through (LVRT) capability is included in the PQ control strategy to support the voltage by supplying reactive power under voltage sag. It is noteworthy to mention that under unbalanced condition negative sequence control loop is used in addition, to control the negative sequence quantities. When the microgrid operates under islanded mode, the reference signals are obtained by controlling the voltage source

inverters as the reference signals cannot be obtained from the grid. In islanded mode of operation, V/f control and droop control strategies are used. A voltage control loop is added whose reference is generated by the voltage for mation loop. The voltage formation loop is different for V/f control and droop control. The required voltage reference and frequency reference are directly given to the voltage formation loop in V/f control whereas in droop control the voltage and frequency references are obtained from droop characteristics of measured active and reactive powers.

3.1.1 Control Scheme for DGs

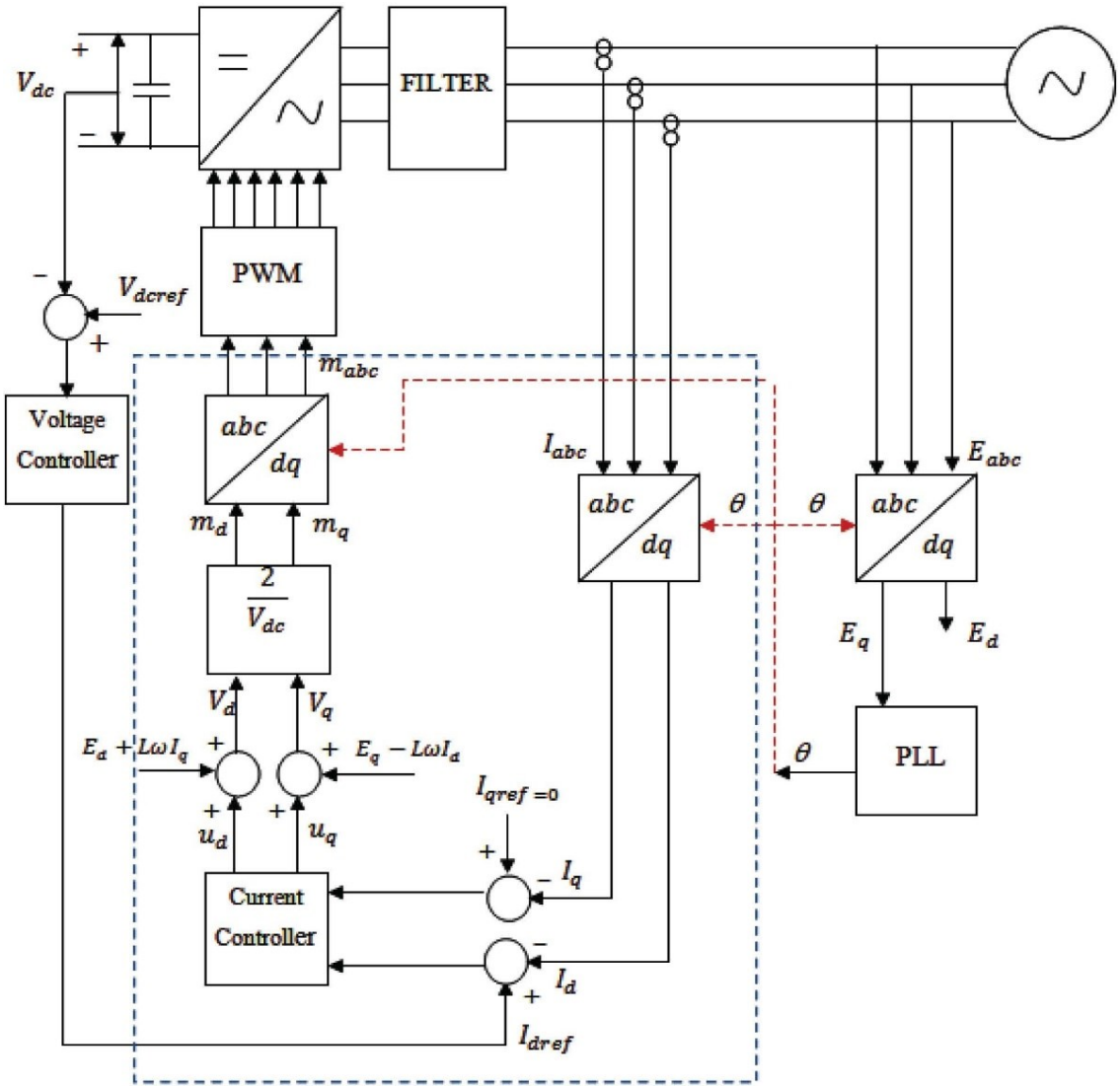

Fig. 3.1 DG converter control scheme

In this study, a synchronous reference frame control is chosen. It is also called as dq control. It uses a reference frame transformation module, abc to dq to transform the grid current and voltage waveforms into a reference frame that rotates synchronously with the grid voltage so that the control variables become dc values. Thus, filtering and controlling can be easily achieved. In the inverter control structure, given in Fig. 3.1, the dc- link voltage is controlled in accordance with the PV or wind output power. Its output acts as reference for the active current controller (I_{d_ref}), whereas the reference for the reactive current controller (I_{q_ref}), is set to zero, as the photovoltaic system connected to low voltage distribution network is expected to deliver only active power under normal scenario. Hence, the current vector is always in phase with the grid voltage. The dq control structure is associated with K factor controllers since they have a satisfactory behaviour while regulating dc variables. The phase angle used for the abc to dq transformation module is obtained by the Phase-Locked Loop (PLL) [65].

In this thesis, the fault detection method is for grid-connected IIDGs, where the IIDGs are under the PQ control strategy. By controlling the change of the active and reactive current reference tracking, the control system can output the given reference value of the active and reactive power, which are described as:

$$\begin{cases} P_{ref} = U_d I_{d\_ref} \\ Q_{ref} = U_d I_{q\_ref} \end{cases} \tag{3.1}$$

where P_{ref} and Q_{ref} are the reference values of the active and reactive powers, U_d is the DG's d-axis voltage at the grid connection point (GCP) and I_{d_ref} and I_{q_ref} are the reference values of the active and reactive currents.

3.1.2 Low Voltage Ride Through (LVRT)

According to the rules of the German grid code [66], PQ-DGs, such as turbine generations (TGs) and photovoltaic power generations (PPGs), in a microgrid should have the LVRT capability, which can improve the voltage level by providing reactive power during a fault. High penetration of the DGs into the grid causes voltage fluctuations at the PCC. To maintain the nominal voltage, the DG inverters operate according to Volt–Var

curve which is a decentralized and autonomous form of voltage control. The Volt-Var curve is usually centered around the nominal voltage. If the voltage is above the set point, the inverter absorbs the reactive power and when the voltage is below the set point the inverter delivers the reactive power. The grid connected DGs have the LVRT capability which delivers the reactive power to support the grid voltage during the voltage sags. The LVRT function should start when the voltage sag exceeds 10%. Fig. 3.2 shows the LVRT requirement of direct grid-connected PQ-DGs [67]; the reactive current profile is given as a solid line.

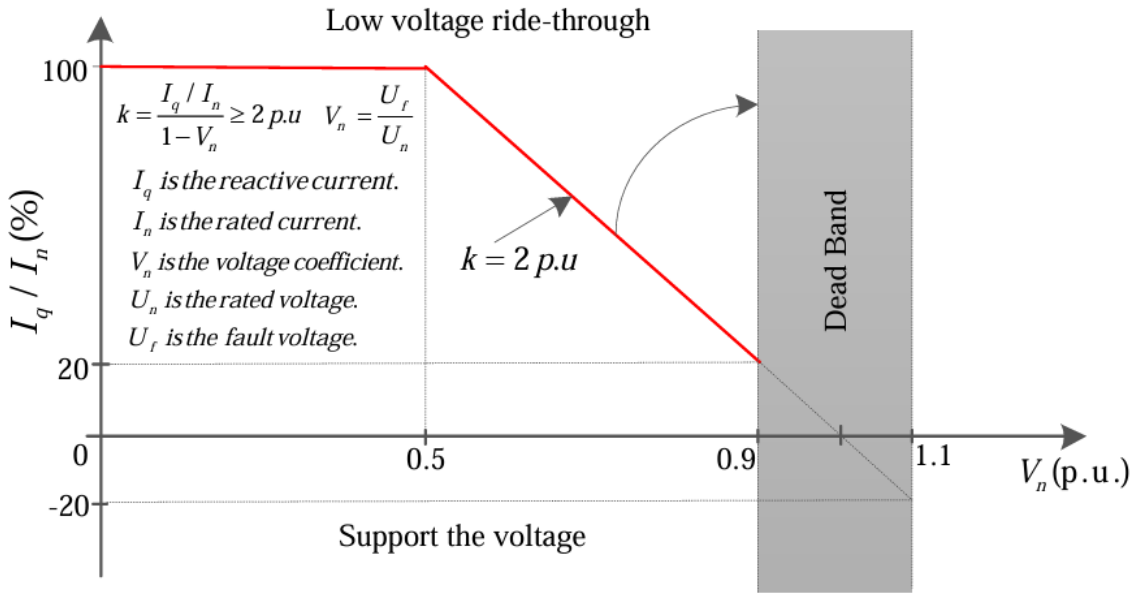

Fig. 3.2 LVRT requirement of direct grid-connected DGs

In Fig. 3.2, for the grid voltage coefficient in the range of 90%~100%, there is no reactive current output of the PQ-DG. For the grid voltage coefficient in the range of 50%~90%, 2% of the reactive current must be provided by the PQ-DG with every 1% voltage drop, and when the grid voltage coefficient falls below 50%, the system should provide a 100% reactive current. The reactive current reaches a maximum value Imax and remains constant. To make full use of the renewable energy in the normal condition [68], currently, TG and PPG systems are designed to operate at unity power factor and produce active power only [69], [70]. Reactive power is avoided due to losses in the inverter, lines and transformers [71]. Therefore, the value of the reactive current is zero in the normal condition. Meanwhile, to improve the output characteristic of a PQ-DG, the positive-sequence control

strategy is generally used [72]. The power output in the AC side of the PQ-DG only has the positive-sequence current when a fault occurs in the microgrid. Thus, the PQ-DG can be equivalent to a positive-sequence current source that is controlled by the grid voltage at the GCP. Therefore, the output reactive fault current can be described as follows:

$$I_q = \begin{cases} 0, & 0.9U_n < U_{d.f}^{+} \leq U_n \\ 2I_{max}\left(1 - \frac{U_{d.f}^{+}}{U_n}\right), & 0.5U_n < U_{d.f}^{+} \leq 0.9U_n \\ I_{max}, & 0 \leq U_{d.f}^{+} \leq 0.5U_n \end{cases} \quad (3.2)$$

where I_q is the output reactive fault current and $U_{d.f}^{+}$ is the d-axis positive-sequence fault voltage of the PQ-DG. The reference current amplitude cannot exceed its maximum permissible value I_{max}, which is usually less than twice of the rated current of the PQ-DG. The amplitude of I_{max} obeys the following principle:

$$\sqrt{I_d^2 + I_q^2} \leq |I_{max}| \quad (3.3)$$

where I_d is the output active fault current. Thus, the output active fault current can be described as follows:

$$I_d = \begin{cases} P_{ref}/U_{d.f}^{+}, & 0.9U_n < U_{d.f}^{+} \leq U_n \\ \min\left(\frac{P_{ref}}{U_{d.f}^{+}}, \sqrt{I_{max}^2 - I_q^2}\right), & 0.5U_n < U_{d.f}^{+} \leq 0.9U_n \\ 0, & 0 \leq U_{d.f}^{+} \leq 0.5U_n \end{cases} \quad (3.4)$$

3.2 PROPOSED MICROGRID TEST SYSTEM:

A basic model of a microgrid, as depicted in Fig. 3.3, is constructed following the IEEE 1547 standard and the overview provided by the Consortium for Electric Reliability Technology Solutions (CERTS). The microgrid model operates in grid-connected mode in which the IIDGs operates in current control mode (PQ-control), where it utilizes the grids voltage and current as reference at the PCC. The test system consists of three loads denoted as LOAD1-LOAD3 and the distributed generators are referred to as DG1 and DG2. The

circuit breakers (CBs) for the feeders are labelled as A1-A4, B1-B3, and C1-C3. The Main feeders, such as L3 and L4, have CBs at both the ends while branch feeders, such as L1, L2, L5, L6, L7, and L8, have CBs placed at upstream.

The microgrid test system comprises two wind-based IIDGs rated at 500 kW and 600 kW, respectively. Each is connected to a main feeder through circuit breakers. The lengths of the feeders are as follows: L1 = 5 km, L2 = 15 km, L3 = 5 km, L4 = 8 km, L5 = 12 km, L6 = 12 km, L7 = 12 km, and L8 = 12 km. L2, L6, and L8 are connected to series RLC loads, while L5 and L7 are connected to IIDGs, and main feeders L3 and L4. Load 1 consists of R1 = 1.4 Ω, L1 = 95.6 H, and C1 = 3.184 μF; load 2 comprises R2 = 1.3 Ω, L2 = 636.95 H, and C2 = 3.184 μF; load 3 includes R3 = 1.4 Ω, L3 = 1019.11 H, and C3 = 3.184 μF. The system operates at a grid frequency of 50 Hz with an operating voltage of 10 kV. The IIDGs supports the LVRT capability, whenever fault occurs for every 1% voltage drop IIDG suplies 2% reactive current when the voltage level is between 90% to 50% and if the voltage level is below 50% it will inject maximum reactive power.

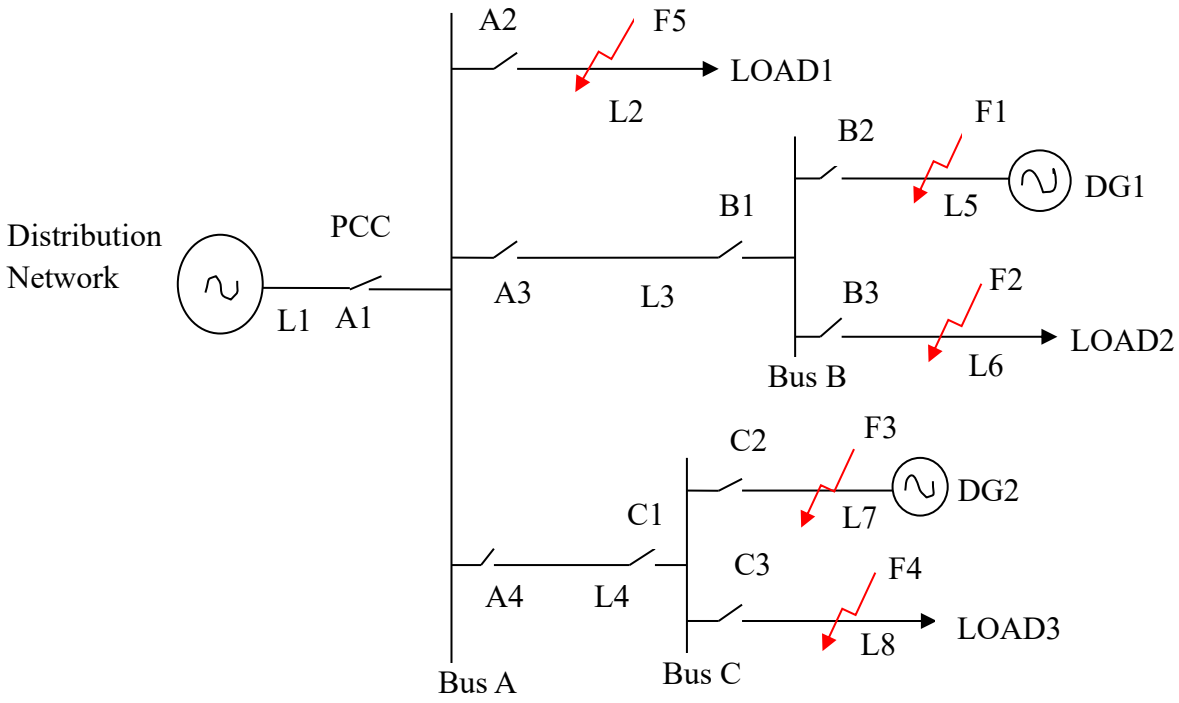

Fig. 3.3 Test model of a microgrid.

CHAPTER – IV

PROPOSED FAULT DETECTION TECHNIQUE

4.1 LISSAJOUS FIGURE

Lissajous figures, named after French mathematician Jules Antoine Lissajous, offer a captivating visual representation of the relationship between harmonic motions. These figures are formed by plotting the positions of two oscillating variables against each other over time. Typically, these variables are sinusoidal functions of different frequencies and phases. When these oscillations are graphed on perpendicular axes, the resulting patterns reveal intricate and mesmerizing curves that hold valuable insights into the underlying harmonic relationships. Mathematically, Lissajous figures are fascinating due to their connection with parametric equations and trigonometric functions. The parametric equations used to generate Lissajous curves involve sine and cosine functions, showcasing the fundamental role of trigonometry in describing periodic motion and waveforms. Analyzing these equations allows mathematicians and physicists to predict and understand the behavior of complex harmonic systems, providing insights into phenomena ranging from mechanical vibrations to electromagnetic waves. These figures find extensive use in physics and engineering, particularly in the study of waveforms and oscillatory systems.

In electrical engineering, Lissajous figures are used in oscilloscopes to analyze the phase relationship between two electrical signals. By displaying one signal on the horizontal axis and another on the vertical axis, engineers can quickly assess whether the signals are in phase, out of phase, or have a specific phase difference, crucial for tasks like tuning circuits and analyzing signal distortions. The formation of Lissajous figures is governed by the relative frequencies, phases, and amplitudes of the two oscillating variables. The frequency ratio between the two motions determines the overall shape of the Lissajous figure, with integer ratios resulting in closed curves and irrational ratios producing more complex, non-repeating patterns. For example, when the frequency ratio is a simple integer like 1:1, the resulting Lissajous figure is a perfect circle. As the ratio deviates, the figure transforms

into ellipses, and further variations lead to intricate patterns such as lemniscates, spirals, and loops.

The Lissajous figures allows to plot one sine wave along the x-axis against another sine wave along the y-axis. The Lissajous figure shows the phase difference between the two signals and the relationship between their frequencies.

In our study, the voltage and current signals collected from the PCC in the microgrid can be graphically represented in the form of a Lissajous curve.

4.1.1 Representation of Lissajous Figures:

A Lissajous curve is a graphic representation of the voltage and current signals that were obtained from each feeder.

The signals for the instantaneous voltage and current are expressed as

$$v = V_o \sin(wt) \tag{4.1}$$

$$i = I_o \sin(wt + \delta) \tag{4.2}$$

where V_o and I_o are the voltage and current signal amplitudes, respectively, and δ is the power factor angle. The voltage signal is placed in the y-axis and the current signal is placed in the x-axis to create the Lissajous figure. Next, we obtain the relationship between waveform v and waveform i by eliminating wt from equations (4.1) and (4.2). Accordingly, from (4.1), we have:

$$wt = \sin^{-1}\left(\frac{v}{V_o}\right) \tag{4.3}$$

By substituting (3) in (2) we can obtain as follows:

$$i = I_o \sin\left(\sin^{-1}\left(\frac{v}{V_o}\right) + \delta\right) \tag{4.4}$$

By applying the trigonometric identities to solve (4.4), (4.5) can be obtained.

$$\frac{i}{I_o} - \frac{v}{V_o}\cos\delta = \sin\delta\sqrt{1 - \left(\frac{v}{V_o}\right)^2} \tag{4.5}$$

Squaring on both sides to (4.5), we can obtain (4.6)

$$\frac{i^2}{I_o^2} - 2\frac{\cos\delta}{I_o V_o} iv + \frac{v^2}{V_o^2} - sin^2\delta = 0 \qquad (4.6)$$

The general equation of 2^{nd} degree is (4.7)

$$Ax^2 + 2Hxy + By^2 + 2Gx + 2Fy + C = 0 \qquad (4.7)$$

By comparing (4.6) and (4.7) we get the values of

$$A = {}^{1}/_{I_o^2}, \qquad H = -\frac{\cos\delta}{I_o V_o}, \qquad B = {}^{1}/_{V_o^2},$$

$$G = 0, \qquad F = 0, \qquad C = -sin^2\delta \qquad (4.8)$$

So, equation (4.6) always represents an ellipse because

$$H^2 - AB < 0 \qquad (4.9)$$

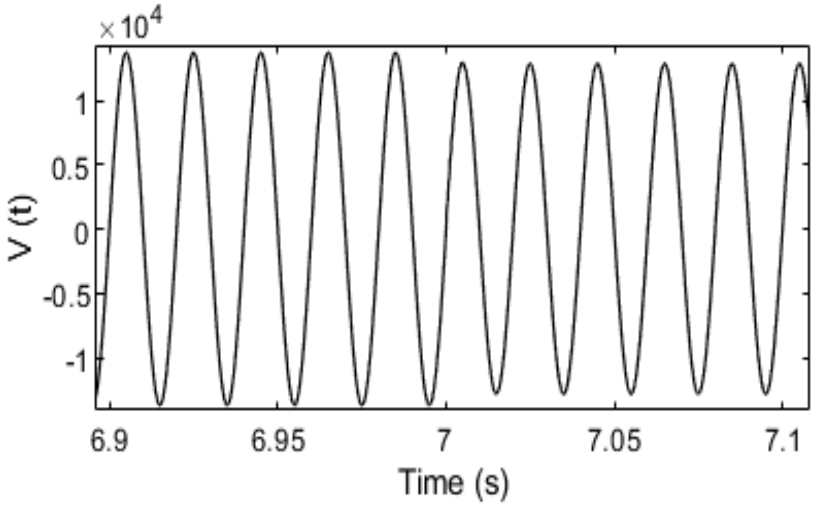

(a)

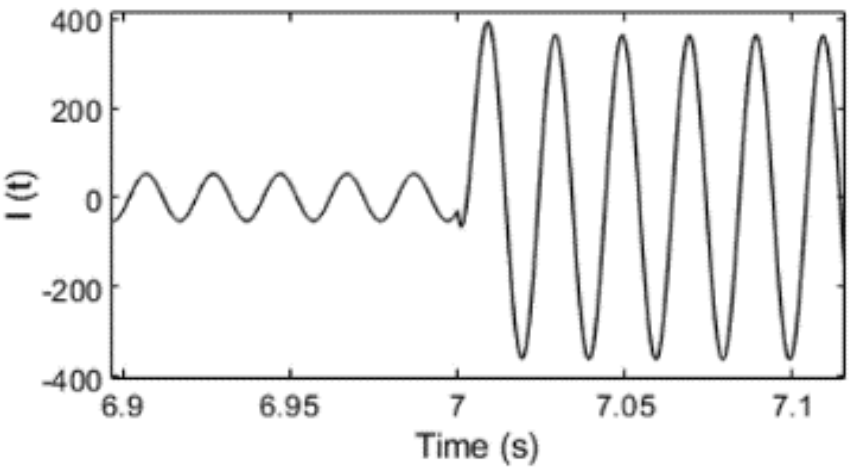

(b)

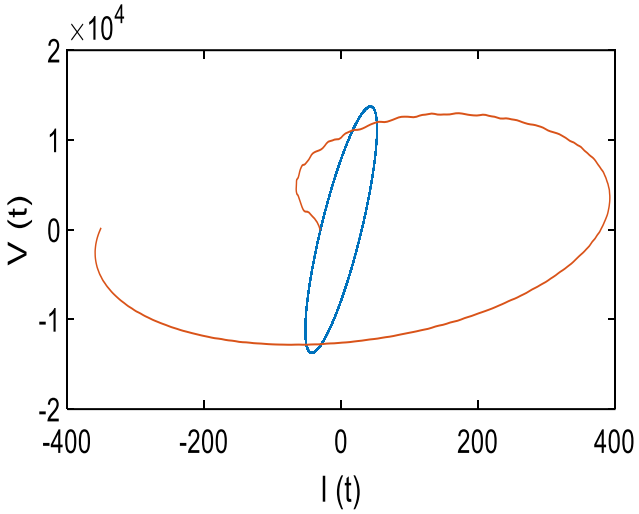

(c)

Fig. 4.1 (a) Voltage signal (b) Current signal (c) Lissajous figure of corresponding voltage and Current signal.

Hence, in Fig. 4.1 under normal operating conditions, the Lissajous curve that is produced based on the v vs i is always an ellipse. The Lissajous figure deviates from its original elliptical shape (blue color) when fault occurs because it disrupts the voltage and current signals at the respective feeder. As a result, under a fault event, the Lissajous figure shape changes (orange colour).

4.2 SIMILARITY INDEX:

The fault detection technique is developed based on the data from WMUs and the associated Lissajous curve. The suggested technique is predicated on changes in the Lissajous curve area during two consecutive cycles.

Let's define the area of the Lissajous curve at time 't' over period T as follows:

$$Area_{v-i}(t) = \left| \int_{i(\tau=t-T)}^{i(\tau=t)} v(\tau) di(\tau) \right| \qquad (4.10)$$

At normal condition the successive areas are almost equal.

For instance, at normal operating condition, if $Area_{v-i}(t)$ is the area at time 't' and $Area_{v-i}(t-\Delta t)$ is the area at time 't-Δt', both will be almost equal, where 'Δt' is the time interval. There will be some variation between the $Area_{v-i}(t)$ and $Area_{v-i}(t-\Delta t)$ if any event happens at time 't'. Thus, in order to identify the fault condition, a similarity index based on the area of the Lissajous figure as illustrated in (4.11) has been developed.

$$SI(t) = 1 - \left| \frac{Area_{v-i}(t) - Area_{v-i}(t-\Delta t)}{max\{Area_{v-i}(t), Area_{v-i}(t-\Delta t)\}} \right| \qquad (4.11)$$

SI(t) is near to one if the areas of the two consecutive Lissajous curves are almost equal. SI(t) comes near to zero when the areas of the two succeeding Lissajous curves differ significantly which indicates that there has been an abrupt change in the Lissajous curve at time 't'. This indicates that fault occurred at time 't'.

3.3 PROPOSED FAULT DETECTION METHOD:

When a fault occurs, the entire microgrid system will be disturbed. Therefore, it is necessary to calculate the Similarity Index (SI) at every Circuit Breaker (CB). By calculating the SI at the CBs and comparing with the threshold we can differentiate between faulty phase and healthy phase and also the fault locations. In the proposed algorithm, two thresholds, T1 and T2, have been considered. T1 is the threshold given to the main feeders and DG feeders while T2 is used for load feeders. By analyzing the SI for all faults at every CB of the microgrid test system as shown in Fig. 3.3, the thresholds have been selected as 0.17 and 0.26 respectively for T1 and T2.

The branch feeders L5, L6, L7 and L8 are connected to the main feeders L3 and L4 therefore any disturbance occurs in the branch feeders will affect the main feeders. Hence the proposed fault detection scheme is initiated by checking the SI at the main feeders as shown in the Fig. 4.2 and explained below.

Case 1: If SI at CB-A3 is less than CB-A4, then check if the SI of CB-A3 is less than T1. If it is less than T1, then the fault is at CB-B2 or CB-B3 (because the feeders L5 and L6 are connected to the main feeder L3). If the SI of CB-B2 is less than T1, then fault is occurred at that CB-B2 or If the SI of CB-B3 is less than T2, then fault is occurred at that CB-B3. If it is not less than T1 and if the SI of CB-A2 is less than T1, then fault is occurred at CB-A2.

Case 2: If SI at CB-A3 is greater than CB-A4, then check if the SI of CB-A4 is less than T1. If it is less than T1, then the fault is at CB-C2 or CB-C3; otherwise, the fault is at CB-A2 (if it is less than T2). If the SI of CB-C2 is less than T1, then fault is occurred at that CB-C2. If the SI of CB-C3 is less than T2, then fault is occurred at that CB-C3.

The proposed method only utilizes the voltage and current signals at each breaker (preferably in p.u) and analyses the waveform behavior and detects the faults hence the size of the DGs doesn't affect the proposed scheme and also it doesn't add any additional disturbance signals into the system. Therefore, it will not lead to power quality issue.

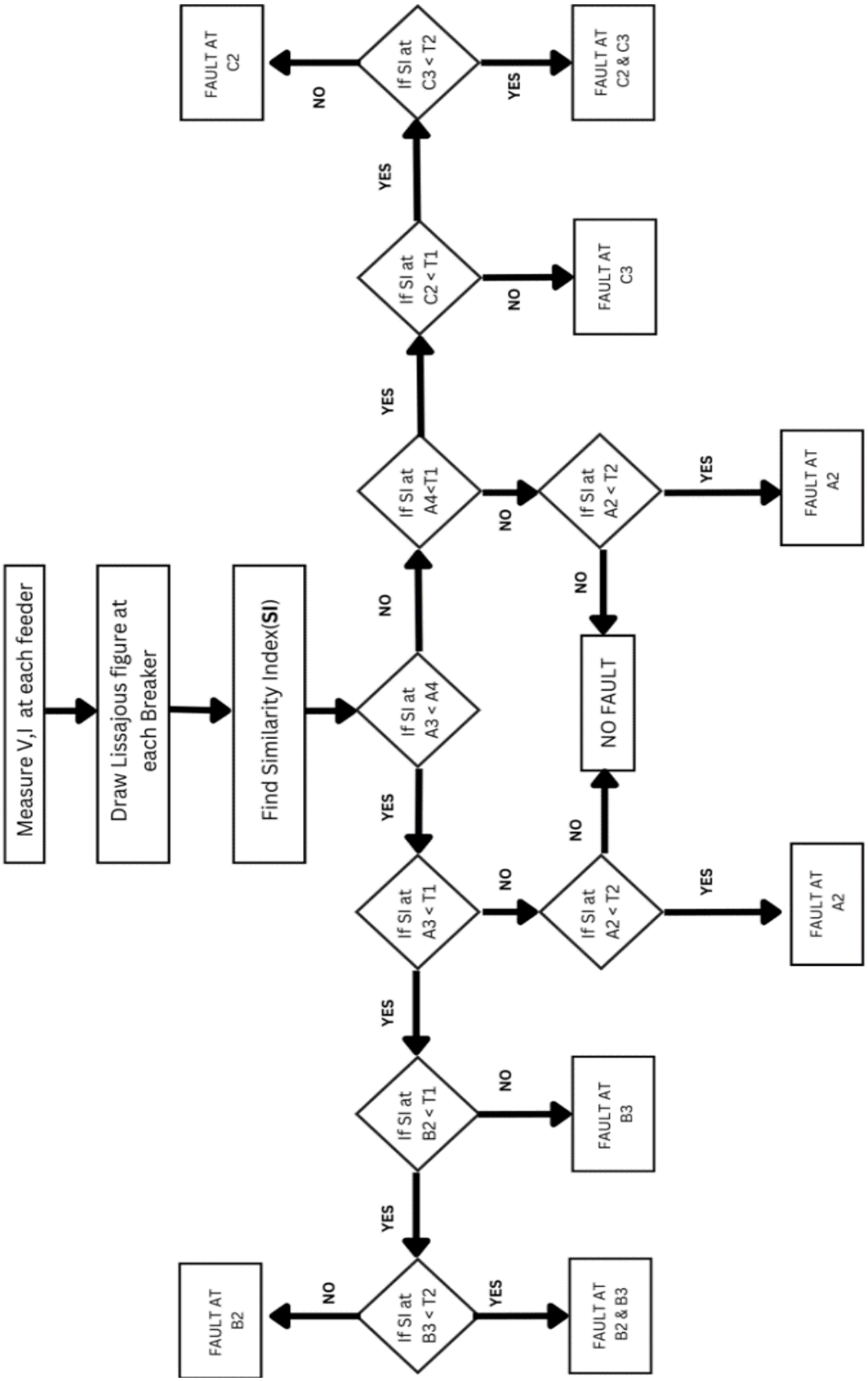

Fig. 4.2 Flowchart and algorithm

CHAPTER – V

SIMULATION RESULTS

5.1 FUNCTIONING OF LVRT:

CASE 1:

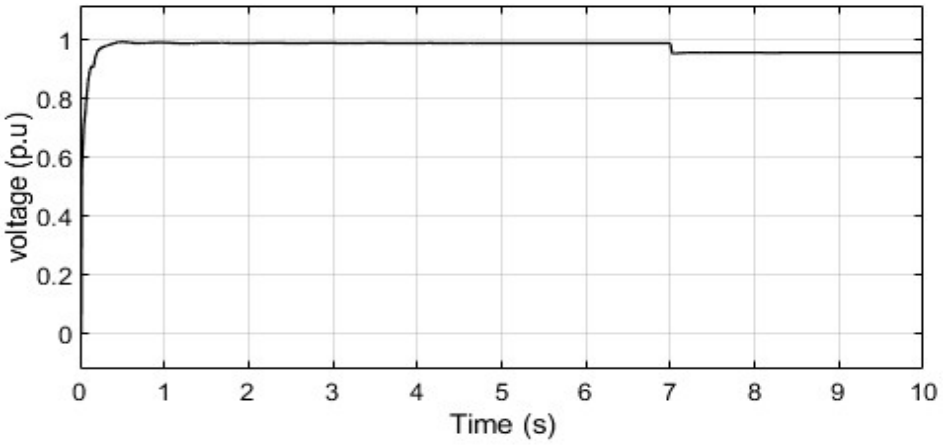

(a)

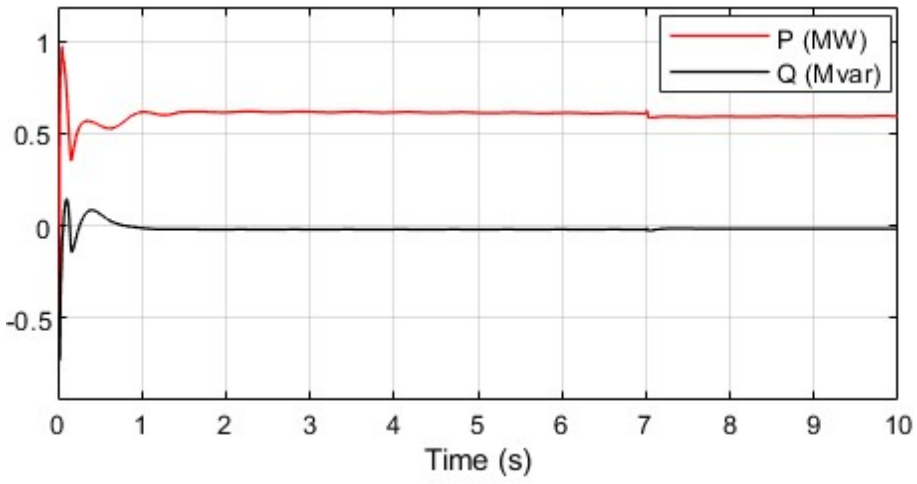

(b)

Fig. 5.1 When LG fault (100 Ω) occurs on L7 feeder at 7 secs: (a) Voltage at DG2 (b) Active and reactive power of DG2.

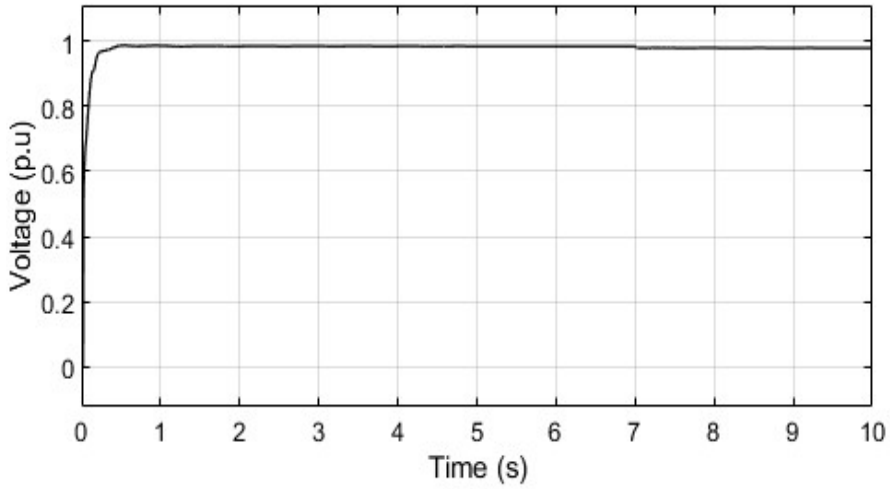

(a)

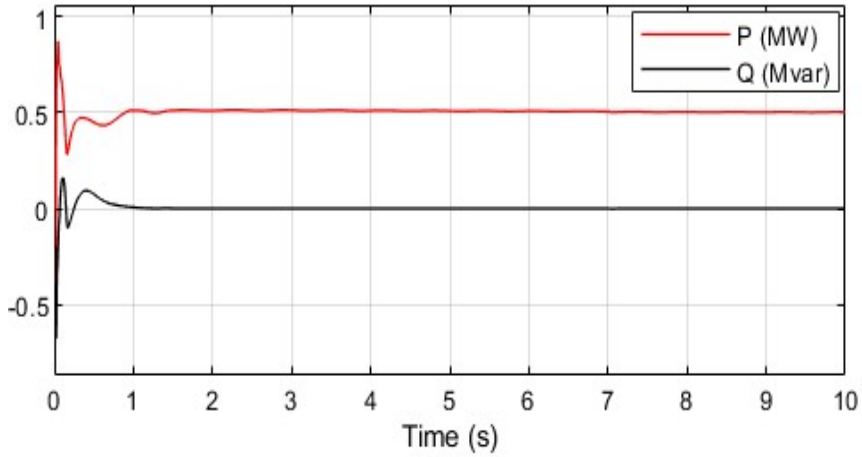

(b)

Fig. 5.2 When LG fault (100 Ω) occurrs on L7 feeder at 7 secs: (a) Voltage at DG1 (b) Active and reactive power of DG1.

In this case, the LG fault is characterized by a Fault resistance (R_{on}) = 100 Ω and Ground resistance (R_g) = 0.01 Ω. The switching times are set between 7 to 10 secs. The LG fault is applied to L7 feeder, which is having DG2. Then the grid voltage coefficient at DG2 is in the range of 90%~100% as observed in Fig. 5.1(a). So, there is no reactive current output of the PQ-DG in Fig. 5.1(b). And the grid voltage coefficient at DG1 is also same as DG1 as seen in Fig. 5.2(a). So, there is no reactive current output of the PQ-DG in Fig. 5.2(b).

CASE 2:

In this case, the LG fault is characterized by a Fault resistance (R_{on}) = 0.1 Ω and Ground resistance (R_g) = 0.01 Ω. The switching times are set between 7 to 10 secs. The LG fault is applied to L7 feeder, which is having DG2. Then the grid voltage coefficient in the range of 50%~90% as observed in Fig. 5.3(a). So, 2% of the reactive current must be provided by the PQ-DG with every 1% voltage drop as in Fig. 5.3(b). And the grid voltage coefficient at DG2 is in the range of 90%~100% as seen in Fig. 5.4(a). So, there is no reactive current output of the PQ-DG in Fig. 5.4(b).

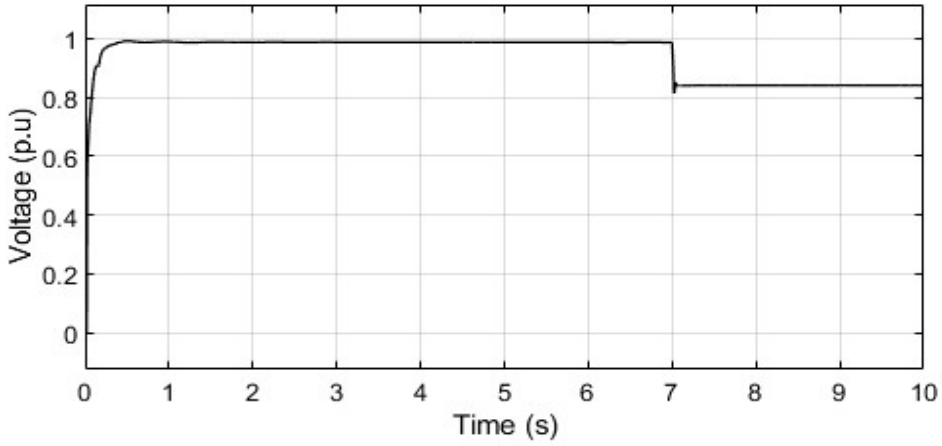

(a)

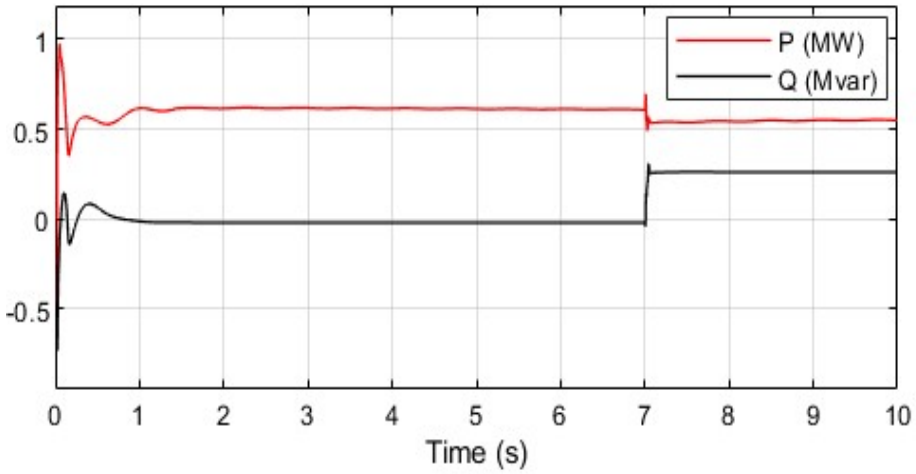

(b)

Fig. 5.3 When LG fault (0.1 Ω) occurrs on L7 feeder at 7 secs: (a) Voltage at DG2 (b) Active and reactive power of DG2.

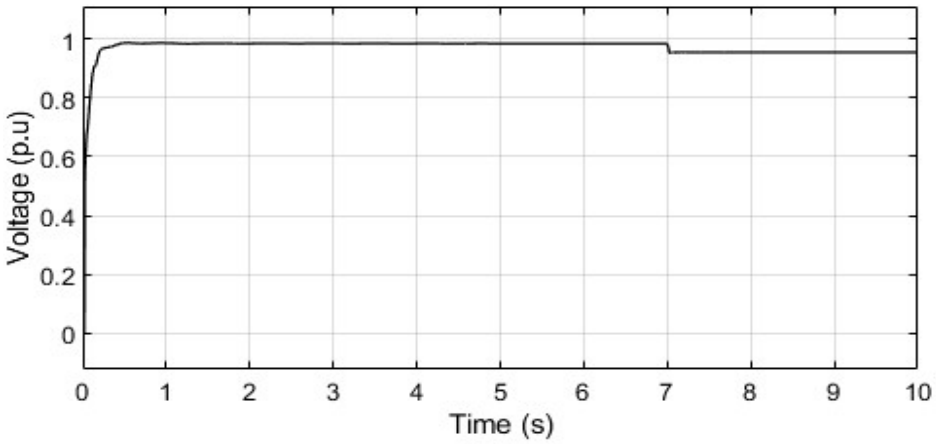

(a)

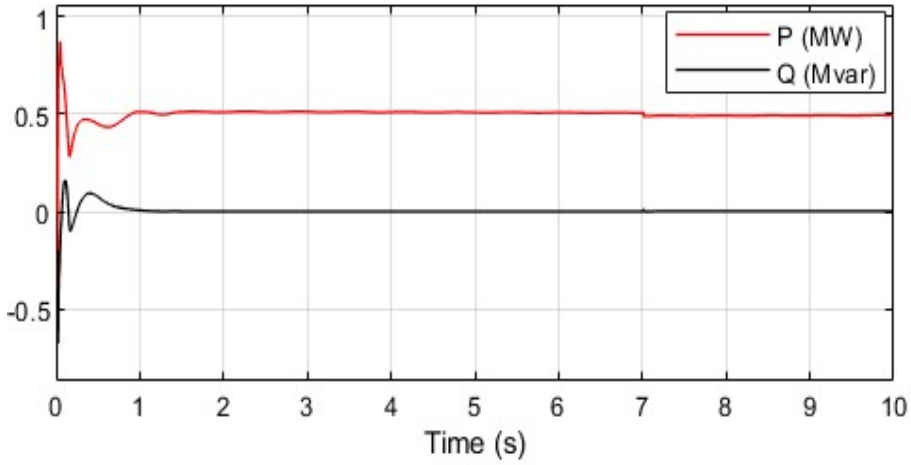

(b)

Fig. 5.4 When LG fault (0.1 Ω) occurrs on L7 feeder at 7 secs: (a) Voltage at DG1 (b) Active and reactive power of DG1.

CASE 3 :

In this case, the LLLG fault is characterized by a Fault resistance (R_{on}) = 10 Ω and Ground resistance (R_g) = 0.01 Ω. The switching times are set between 7 to 10 secs. The LLLG fault is applied to L7 feeder, which is having DG2. Then the grid voltage coefficient falls below 50% as observed in Fig. 5.5(a). So, the system should provide a 100% reactive current and reactive current reaches a maximum value I_{max} and remains constant as in Fig. 5.5(b). And the grid voltage coefficient in the range of 50%~90% as seen in Fig. 5.6(a).

So, 2% of the reactive current must be provided by the PQ-DG with every 1% voltage drop as in Fig. 5.6(b).

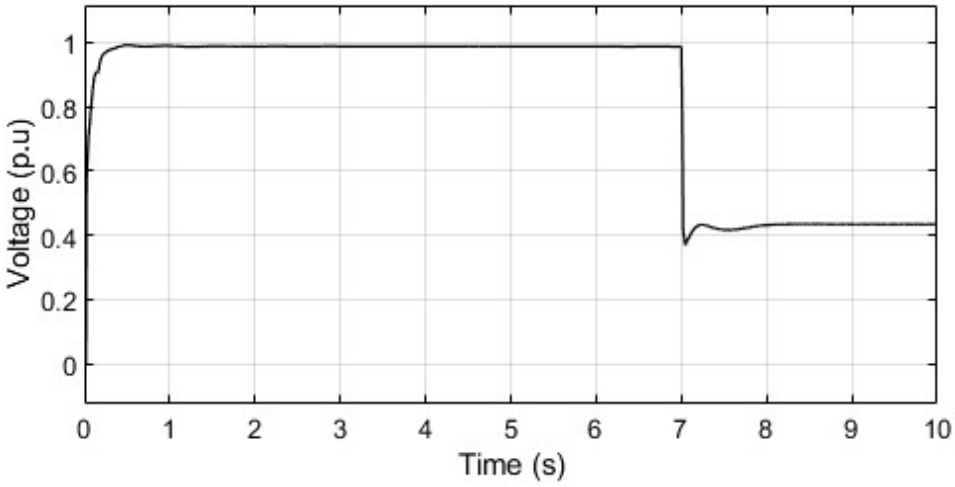

(a)

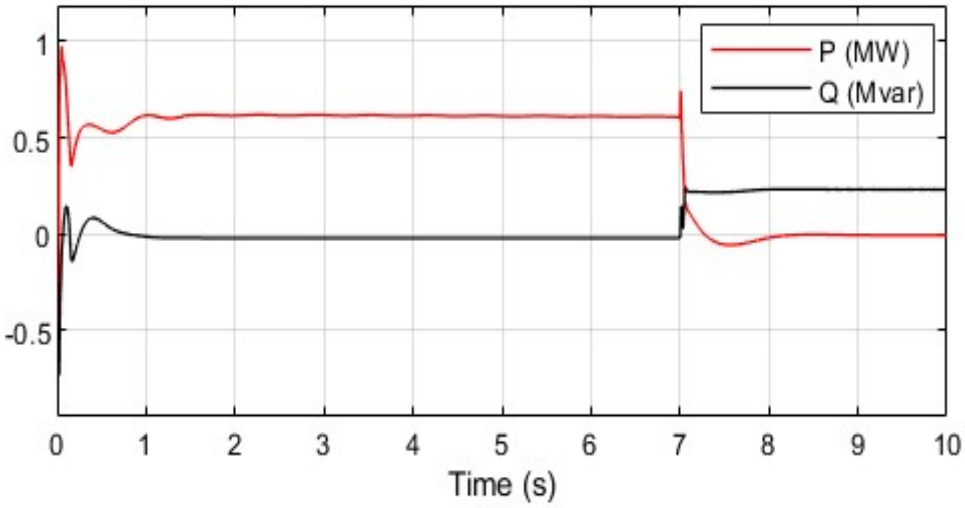

(b)

Fig. 5.5 When LLLG fault (10 Ω) occurs on L7 feeder at 7 secs: (a) Voltage at DG1 (b) Active and reactive power of DG1.

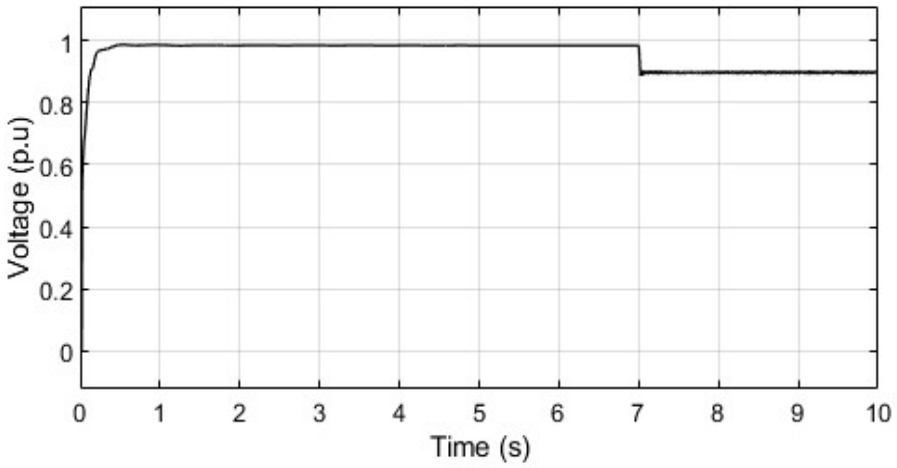

(a)

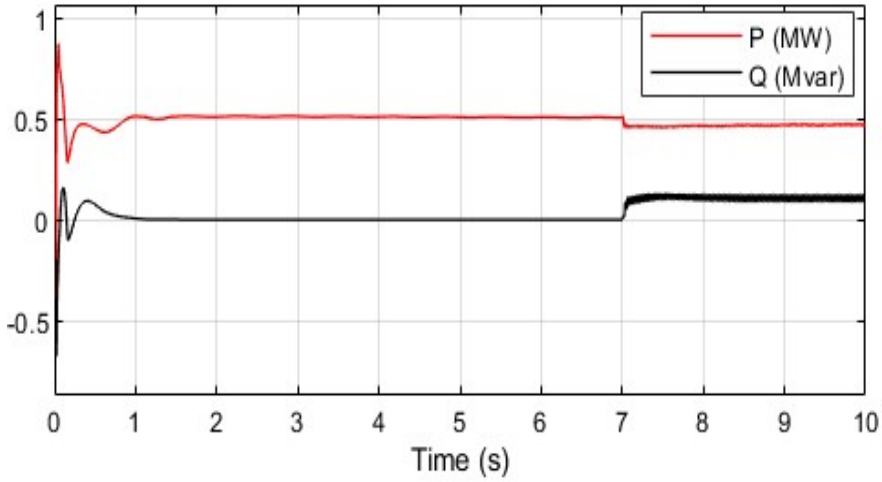

(b)

Fig. 5.6 When LLLG fault (10 Ω) occurs on L7 feeder at 7 secs: (a) Voltage at DG1 (b) Active and reactive power of DG1.

5.2 IDENTIFYING DIFFERENT TYPE OF FAULTS

The proposed fault detection method has been validated for the test system shown in Fig. 3.3 in the MATLAB\Simulink environment. The fault leads the feeder currents and voltages to disturbance, therefore the variations in phase and magnitude of three phases of the feeders has been observed. In this study different asymmetrical and symmetrical faults are considered such as LG, LL, LLG, LLL and LLLG.

5.2.1 Line to Ground Fault (LG)

A single line to ground fault typically happens when one conductor touches the neutral conductor or falls to the ground. In our study, the LG fault is characterized by a Fault resistance (R_{on}) = 0.1 Ω and Ground resistance (R_g) = 0.01 Ω. The switching times are set between 7 to 10 secs. The LG fault is applied to L5 feeder, which is having DG1. The obtained SI values at different CBs are given in Fig. 5.7. When a fault occurs in a branch feeder, the main feeder associated with the same branch feeder is more affected by the fault compared to other main feeders. In this case, as it is a LG fault at L5, the SI for a single phase at CB-A3 and CB-B2 only becomes less the threshold, as observed in Fig. 5.7 (b) and 5.7(d), which is not true at any other CB therefore the proposed method detects the

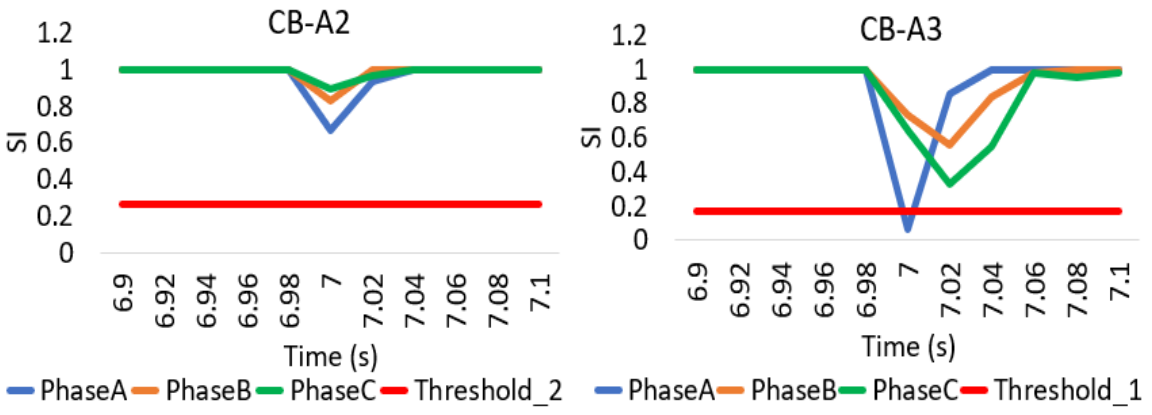

(a)

(b)

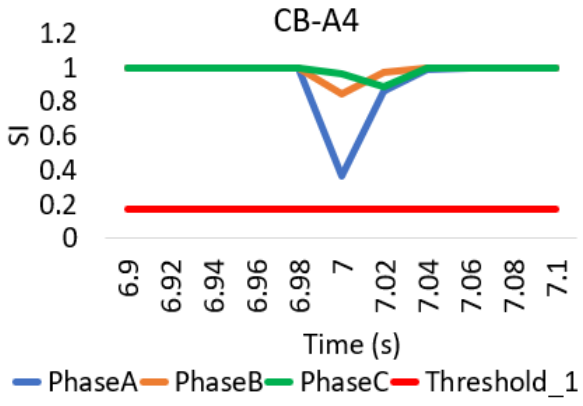

(c)

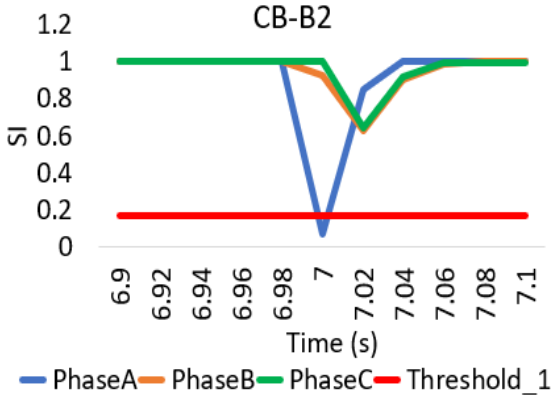

(d)

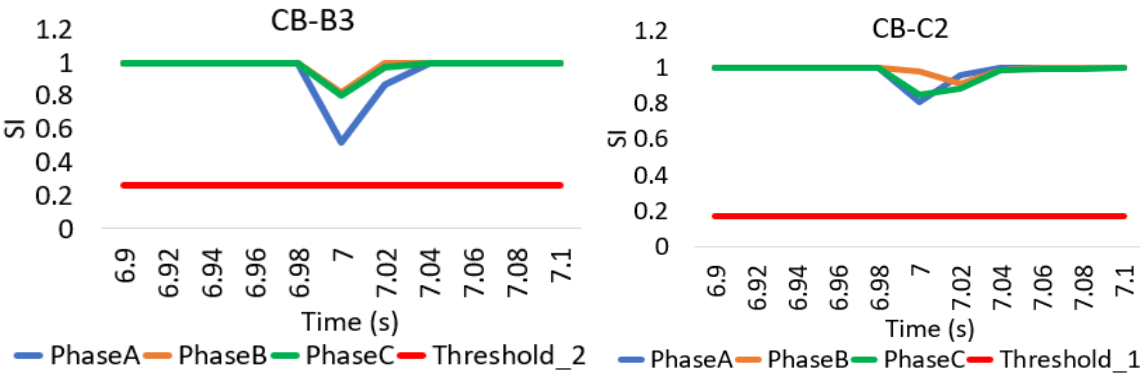

(e)

(f)

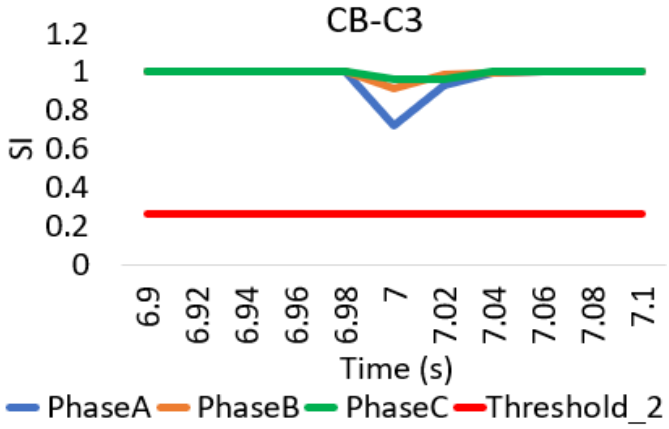

(g)

Fig. 5.7 When LG Fault occur on CB-B2 at 7 secs: (a) SI values at CB-A2, (b) SI values at CB-A3, (c) SI values at CB-A4, (d) SI values at CB-B2, (e) SI values at CB-B3, (f) SI values at CB-C2, (g) SI values at CB-C3.

fault at CB-B2 which is true. The obtained results for LG fault at other locations given in Table 5.1, which displays the similarity index (SI) of all circuit breakers (CBs) when a LG fault occurs, affecting only a single phase.

5.2.2 Line to Line Fault (LL)

A LL fault occurs when two lines are short-circuited. The LL fault is characterized by a Fault resistance (R_{on}) = 0.1 Ω, and switching times between 7 to 10 secs. In Fig. 5.8, The SI values at different CBs are given when a LL fault occurs at L5. The Results shows that the SI for two phases becomes less than the threshold since it is a LL fault, while the remaining feeders are not significantly affected. Table 5.2 indicates the results for LL fault

at different locations, and the results shows that the proposed method can identify the faults accurately. Table 5.2 will also show the SI of all CBs when a LL fault occurs, affecting two phases of the feeders.

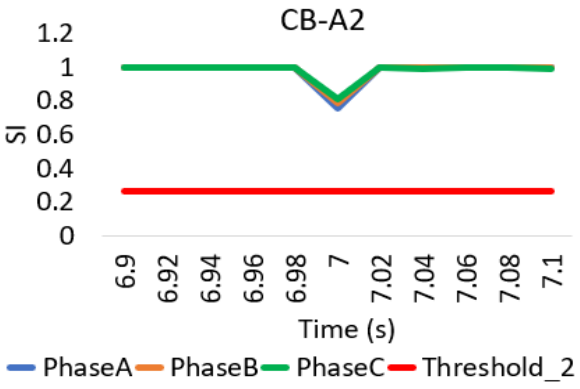

(a)

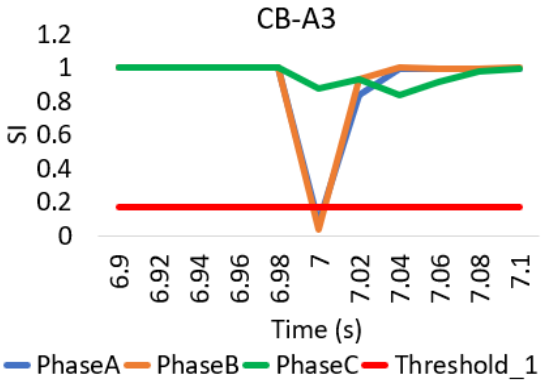

(b)

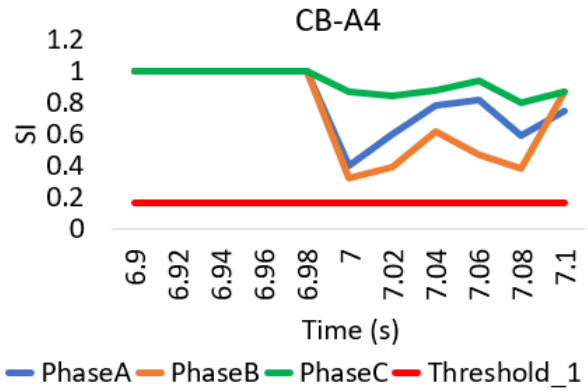

(c)

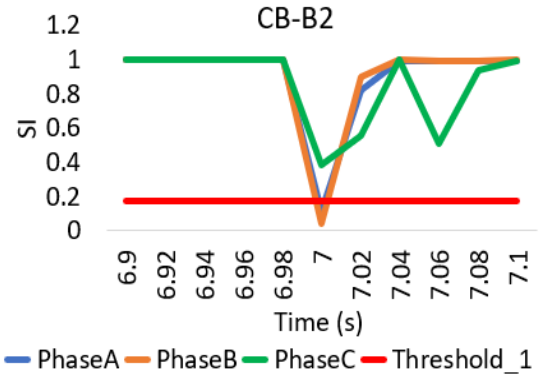

(d)

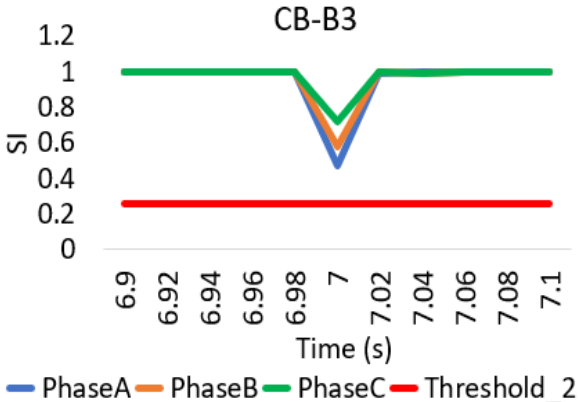

(e)

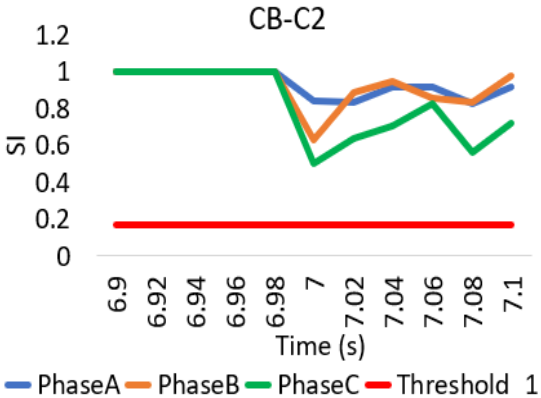

(f)

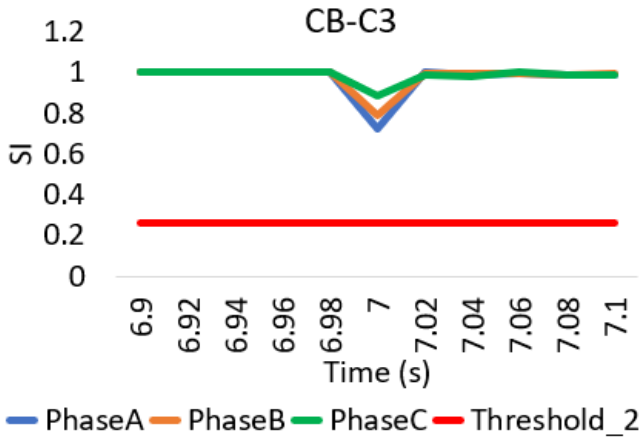

(g)

Fig. 5.8 When LL Fault occur on CB-B2 at 7 secs: (a) SI values at CB-A2, (b) SI values at CB-A3, (c) SI values at CB-A4, (d) SI values at CB-B2, (e) SI values at CB-B3, (f) SI values at CB-C2, (g) SI values at CB-C3.

5.2.3 Double Line to Line Ground (LLG)

A LLG fault occurs when two lines come in contact with each other along with the ground. The LLG fault considered at L6 which is characterized by a Fault resistance (R_{on}) = 0.1 Ω, Ground resistance (R_g) = 0.01 Ω, and switching times between 7 to 10 secs. The Obtained SI values at different CBs has been depicted in Fig. 5.9. Since it is a LLG fault, resulting the SI value for two phases has become less than the thresholds (SI at CB-A3<T1 and SI at CB-B3<T2), while the remaining feeders are not significantly affected. The LLG faults are considered at different locations and the results are given in Table 5.3, which presents the SI of all CBs when a LLG fault occurs, affecting two phases of the feeders.

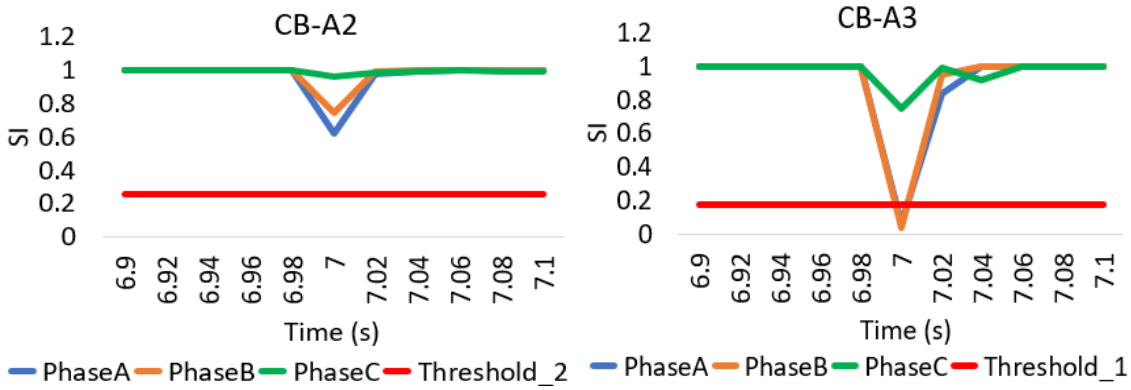

(a) (b)

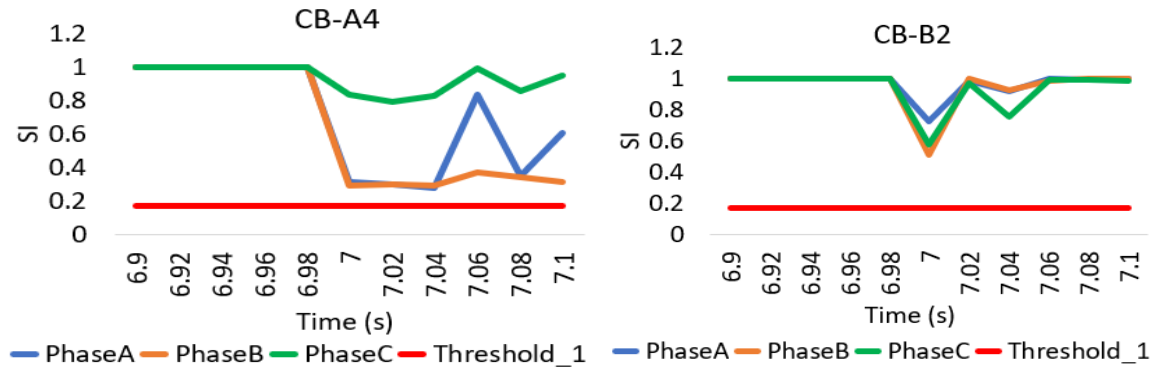

(c)

(d)

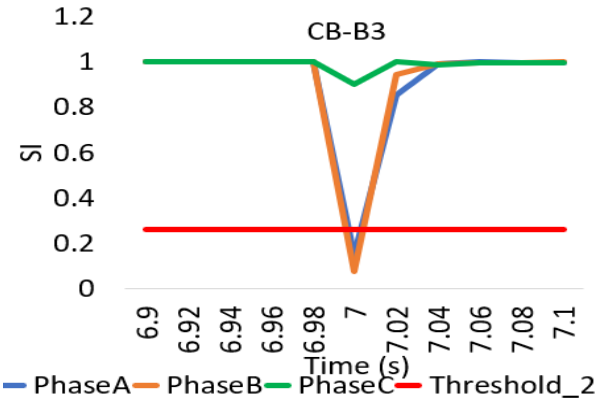

(e)

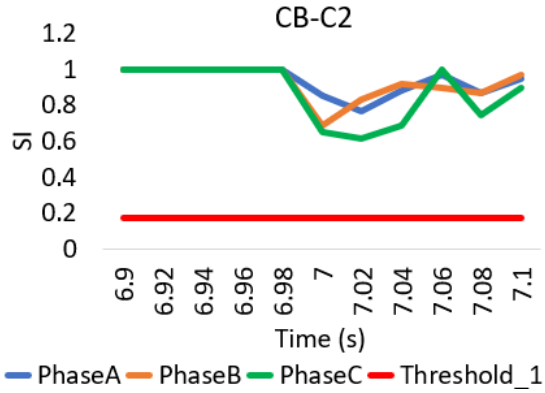

(f)

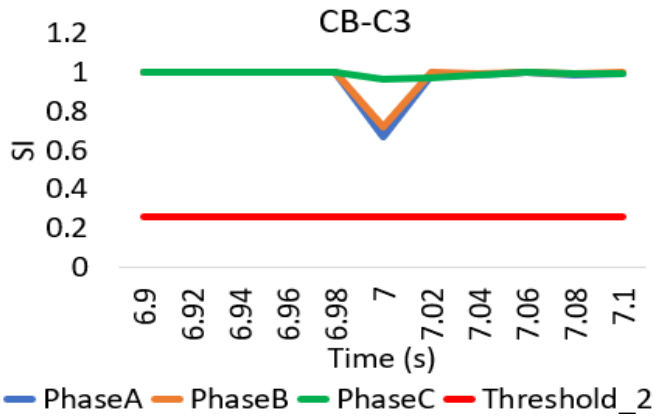

(g)

Fig. 5.9 When LLG Fault occur on CB-B3 at 7 secs: (a) SI values at CB-A2, (b) SI values at CB-A3, (c) SI values at CB-A4, (d) SI values at CB-B2, (e) SI values at CB-B3, (f) SI values at CB-C2, (g) SI values at CB-C3.

5.2.4 Line to Line to Line Fault (LLL) and Line to Line to Line Ground Fault (LLLG)

These are symmetrical faults. Both faults are characterized by a Fault resistance (R_{on}) = 0.1 Ω, and switching times between 7 to 10 secs. Additionally, for LLLG fault Ground resistance (R_g) = 0.01 Ω is also considered. In Fig. 5.10, the SI values when LLL occurs at L5 are given. In this case, the SI for all the three phases have become less than the threshold, while the remaining feeders are not significantly affected. Therefore, the proposed method identifies this as a LLL fault. It is observed that LLLG fault also gives the same results. Table 5.4 gives the information of LLL and LLLG faults at different locations. Providing the SI of all CBs when both an LLLG and LLL fault occur, affecting all the three phases of the feeders.

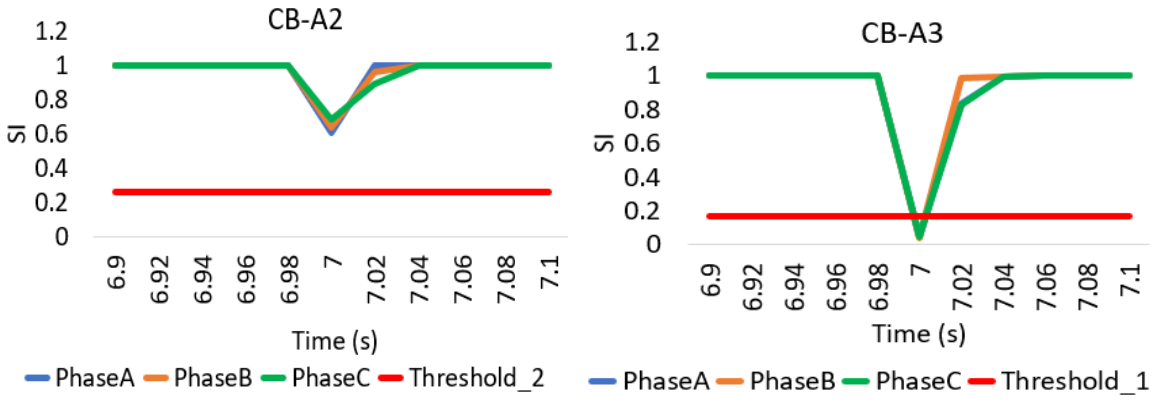

(a)

(b)

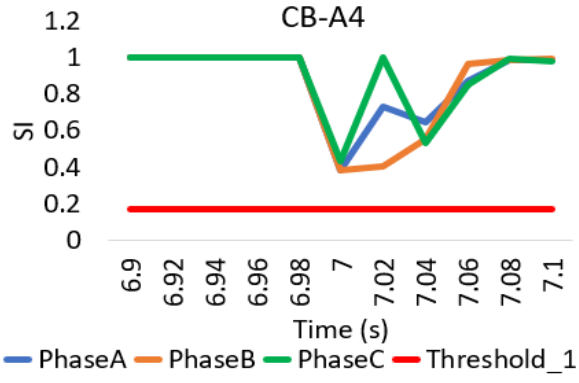

(c)

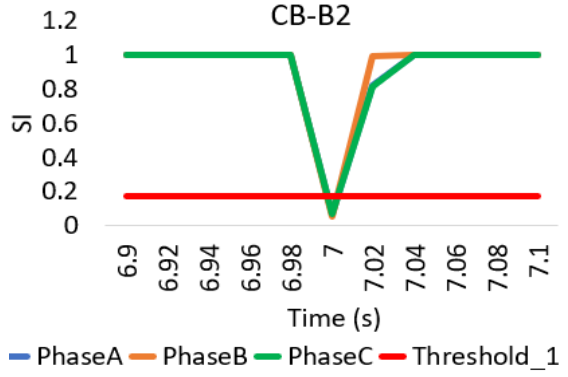

(d)

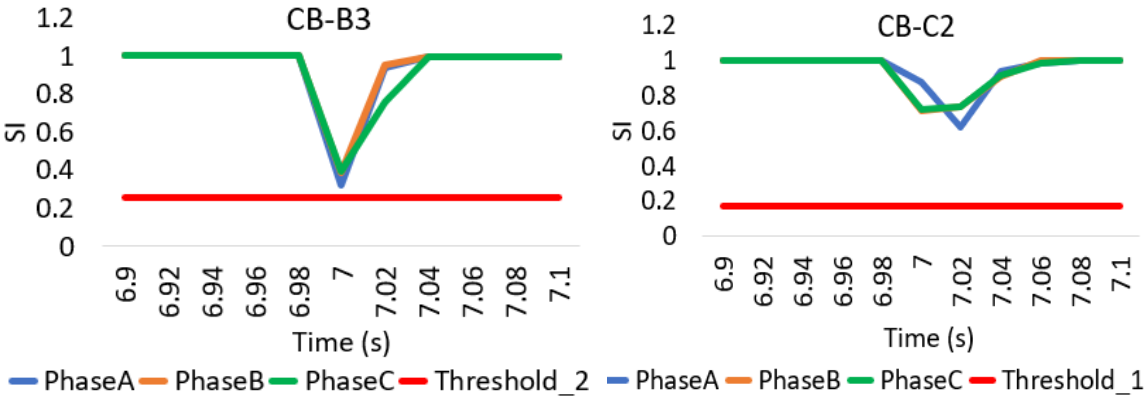

(e)

(f)

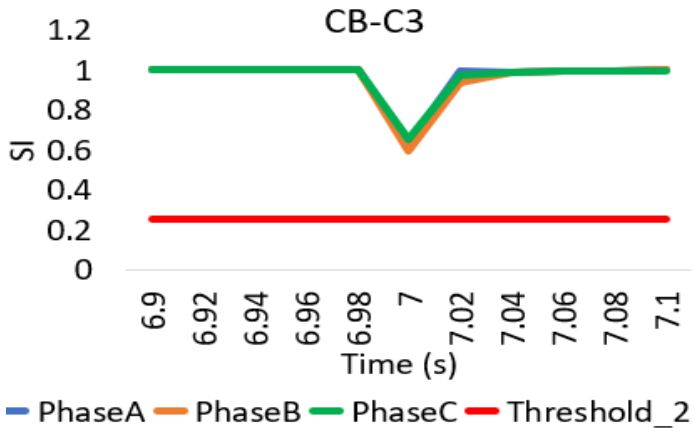

(g)

Fig. 5.10 When LLLG Fault occur on CB-B2 at 7 secs: (a) SI values at CB-A2, (b) SI values at CB-A3, (c) SI values at CB-A4, (d) SI values at CB-B2, (e) SI values at CB-B3, (f) SI values at CB-C2, (g) SI values at CB-C3.

Fault Location	SI at CB-A2			SI at CB-A3			SI at CB-A4			SI at CB-B2			SI at CB-B3			SI at CB-C2			SI at CB-C3		
	Phases			*Phases*			*Phases*			*Phases*			*Phases*			*Phases*			*Phases*		
	A	*B*	*C*	*A*	*B*	*C*	*A*	*B*	*C*	*A*	*B*	*C*	*A*	*B*	*C*	*A*	*B*	*C*	*A*	*B*	*C*
CB-A2	**0.10**	0.63	0.70	0.32	0.81	0.95	0.43	0.87	0.95	0.82	0.94	0.86	0.74	0.91	0.95	0.81	0.95	0.86	0.76	0.94	0.97
CB-B2	0.66	0.82	0.89	**0.06**	0.73	0.64	0.36	0.84	0.96	**0.07**	0.92	0.99	0.52	0.81	0.79	0.80	0.97	0.84	0.72	0.91	0.96
CB-B3	0.67	0.85	0.90	**0.06**	0.52	0.77	0.37	0.86	0.96	0.83	0.91	0.70	**0.12**	0.70	0.70	0.79	0.96	0.85	0.73	0.92	0.95
CB-C2	0.73	0.85	0.92	0.40	0.82	0.97	**0.11**	0.83	0.72	0.86	0.98	0.88	0.76	0.90	0.95	**0.09**	0.87	0.99	0.54	0.85	0.82
CB-C3	0.71	0.86	0.91	0.33	0.82	0.97	**0.10**	0.61	0.86	0.83	0.96	0.86	0.74	0.91	0.95	0.60	0.93	0.65	**0.16**	0.74	0.72

Table 4.1 SI of all CBs when LG fault occurs at 7secs

Fault Location	SI at CB-A2			SI at CB-A3			SI at CB-A4			SI at CB-B2			SI at CB-B3			SI at CB-C2			SI at CB-C3		
	Phases			*Phases*			*Phases*			*Phases*			*Phases*			*Phases*			*Phases*		
	A	*B*	*C*	*A*	*B*	*C*	*A*	*B*	*C*	*A*	*B*	*C*	*A*	*B*	*C*	*A*	*B*	*C*	*A*	*B*	*C*
CB-A2	**0.11**	**0.06**	0.84	0.42	0.34	0.86	0.49	0.42	0.88	0.86	0.74	0.59	0.77	0.82	0.88	0.85	0.71	0.57	0.77	0.83	0.90
CB-B2	0.75	0.78	0.81	**0.07**	**0.03**	0.87	0.40	0.22	0.86	**0.11**	**0.04**	0.38	0.46	0.58	0.72	0.84	0.63	0.50	0.72	0.79	0.88
CB-B3	0.77	0.79	0.82	**0.07**	**0.04**	0.87	0.43	0.31	0.87	0.70	0.48	0.33	**0.17**	**0.08**	0.73	0.85	0.66	0.52	0.73	0.80	0.88
CB-C2	0.81	0.83	0.85	0.53	0.33	0.86	**0.12**	**0.06**	0.86	0.93	0.73	0.62	0.79	0.83	0.90	**0.16**	**0.05**	0.18	0.45	0.58	0.76
CB-C3	0.80	0.82	0.84	0.47	0.32	0.86	**0.11**	**0.06**	0.87	0.90	0.73	0.60	0.78	0.82	0.88	0.68	0.41	0.19	**0.25**	**0.11**	0.73

Table 4.2 SI of all CBs when LL fault occurs at 7secs

Fault Location	SI at CB-A2			SI at CB-A3			SI at CB-A4			SI at CB-B2			SI at CB-B3			SI at CB-C2			SI at CB-C3		
	Phases			*Phases*			*Phases*			*Phases*			*Phases*			*Phases*			*Phases*		
	A	*B*	*C*	*A*	*B*	*C*	*A*	*B*	*C*	*A*	*B*	*C*	*A*	*B*	*C*	*A*	*B*	*C*	*A*	*B*	*C*
CB-A2	**0.09**	**0.06**	0.92	0.27	0.22	0.79	0.39	0.31	0.83	0.88	0.76	0.66	0.69	0.75	0.97	0.87	0.73	0.65	0.70	0.74	0.97
CB-B2	0.59	0.74	0.95	**0.06**	**0.03**	0.94	0.27	0.11	0.81	**0.08**	**0.03**	0.73	0.32	0.50	0.83	0.85	0.64	0.61	0.64	0.71	0.97
CB-B3	0.61	0.74	0.96	**0.06**	**0.03**	0.74	0.31	0.19	0.83	0.72	0.51	0.57	**0.14**	**0.07**	0.89	0.85	0.68	0.64	0.67	0.72	0.96
CB-C2	0.68	0.80	0.97	0.38	0.29	0.80	**0.10**	**0.06**	0.94	0.95	0.76	0.69	0.70	0.78	0.98	**0.12**	**0.05**	0.71	0.34	0.49	0.85
CB-C3	0.66	0.77	0.97	0.31	0.23	0.80	**0.09**	**0.06**	0.79	0.91	0.75	0.68	0.69	0.75	0.97	0.70	0.44	0.52	**0.21**	**0.10**	0.87

Table 4.3 SI of all CBs when LLG fault occurs at 7secs

Fault Location	SI at CB-A2			SI at CB-A3			SI at CB-A4			SI at CB-B2			SI at CB-B3			SI at CB-C2			SI at CB-C3		
	Phases			*Phases*			*Phases*			*Phases*			*Phases*			*Phases*			*Phases*		
	A	*B*	*C*	*A*	*B*	*C*	*A*	*B*	*C*	*A*	*B*	*C*	*A*	*B*	*C*	*A*	*B*	*C*	*A*	*B*	*C*
CB-A2	**0.08**	**0.06**	**0.07**	0.33	0.18	0.28	0.42	0.24	0.36	0.94	0.81	0.81	0.68	0.67	0.73	0.93	0.78	0.79	0.69	0.67	0.72
CB-B2	0.60	0.63	0.68	**0.04**	**0.04**	**0.04**	0.27	0.07	0.23	**0.06**	**0.05**	**0.06**	0.32	0.28	0.39	0.87	0.71	0.72	0.63	0.59	0.65
CB-B3	0.63	0.65	0.70	**0.05**	**0.04**	**0.05**	0.33	0.13	0.27	0.83	0.69	0.66	**0.12**	**0.10**	**0.12**	0.89	0.73	0.74	0.65	0.63	0.68
CB-C2	0.69	0.71	0.75	0.41	0.19	0.29	**0.08**	**0.06**	**0.08**	0.97	0.81	0.82	0.70	0.66	0.69	**0.09**	**0.07**	**0.09**	0.33	0.27	0.39
CB-C3	0.67	0.69	0.74	0.35	0.16	0.27	**0.07**	**0.06**	**0.07**	0.95	0.80	0.79	0.69	0.66	0.69	0.80	0.60	0.57	**0.18**	**0.15**	**0.18**

Table 4.4 SI of all CBs when LLLG, LLL fault occurs at 7secs

5.3 HARDWARE- IN-THE-LOOP TESTING

Through the use of a real-time simulator and an HIL simulation, comparable hardware dynamics are created; indirectly, this results in the creation of a virtual plant that replicates genuine hardware. As a result, the suggested approach has been verified for real-time applications through HIL testing. The four components of the HIL testing setup taken into consideration in this study are as follows:1) Real Time Digital Simulator (RTDS), an industrial standard HIL testing apparatus that simulates the proposed system in real time; 2) RT Lab software, which is used to run the simulation in real time digital simulator. 3) Computer unit, which operates the RT lab, maintains the measurement data, and runs the

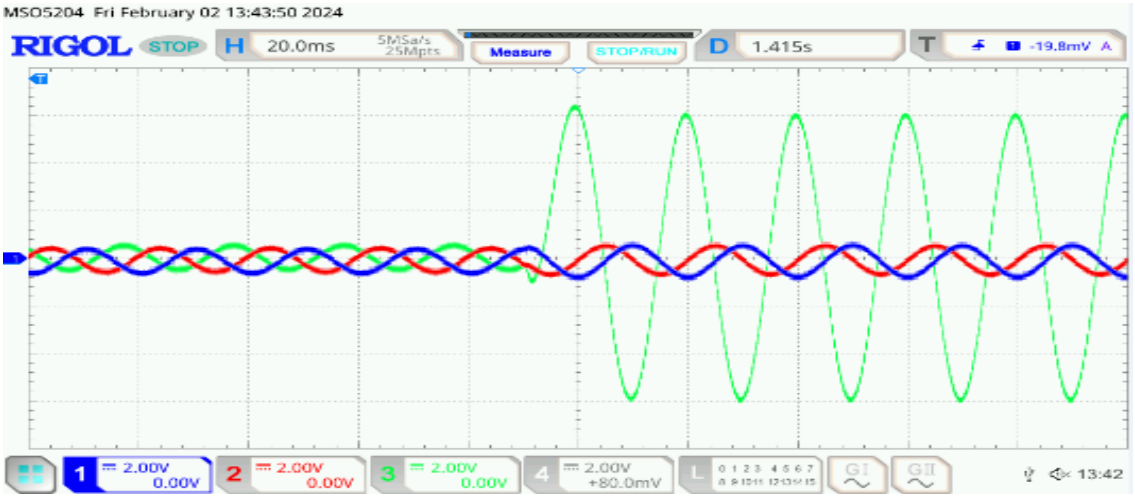

(a)

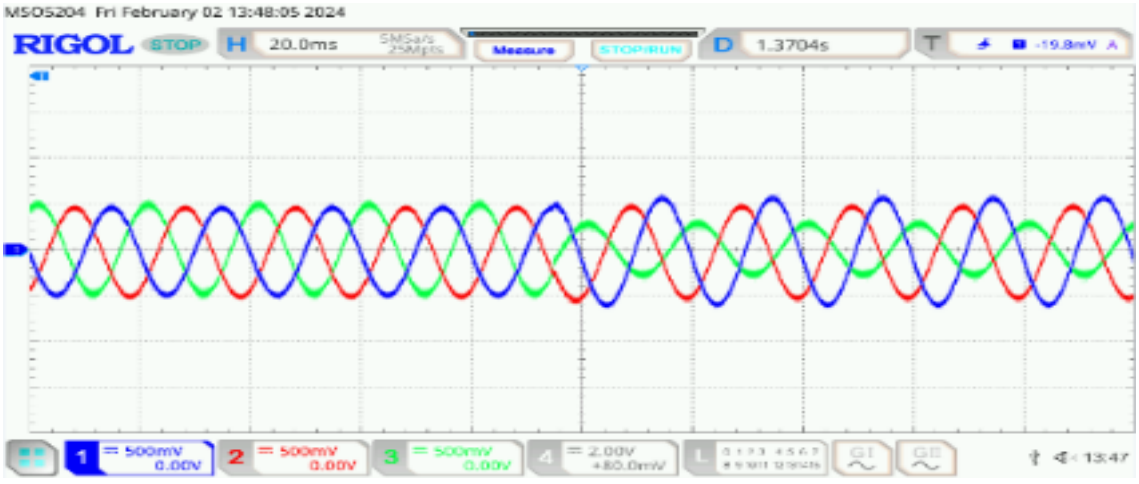

(b)

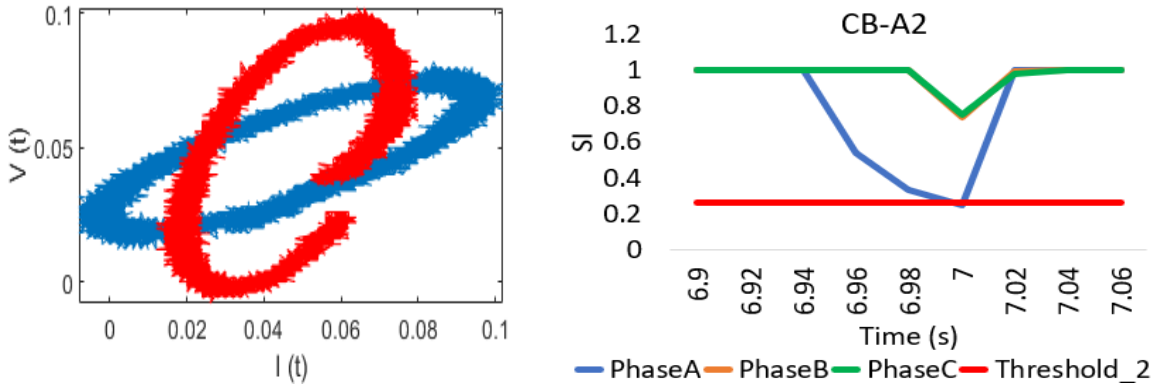

(c) (d)

Fig. 5.11 HIL testing results of fault detection at CB-A2: (a) Current signal, (b) Voltage signal, (c) Lissajous figure of corresponding voltage and Current signal, (d) SI values at CB-A2.

algorithm; 4) Multi channel digital oscilloscope, which serves as the external waveform measurement unit (WMU) hardware to store and record the waveform data. To verify the feasibility of the proposed technique in real-time applications, the test model presented in Fig. 3.3 has been simulated in RTDS using the RT lab software, when LG fault occurs at CB-A2.

To draw the Lissajous figure and to calculate the similarity index, the voltage and current signals are obtained from the digital oscilloscope at each circuit breaker. In Fig. 5.11 (a) and (b), the current and voltage signals are shown before and after the occurrence of the LG fault, while in Fig. 5.11 (c) and (d), the corresponding Lissajous figure and SI at CB-A2 are shown. From the results it can be seen that SI for One phase is becomes below the threshold value at CB-A2 which is not observed elsewhere hence the proposed method detects it as a fault at feeder L2 which is true.

The proposed method is able to detect all kinds of the faults in very less time (0.02s) which allows the microgrid system to isolate the faulty section from the system in less time. Hence the operation of the DGs will not be affected severely therefore the stability of the system will be more.

CHAPTER – VI

CONCLUSION AND FUTURE SCOPE

This study introduces a new approach for identifying low impedance faults within a microgrid by using Lissajous figure patterns. These patterns are created by plotting the voltage and current waveforms of electrical signals against each other. By analyzing the unique characteristics of these Lissajous figures at different circuit breakers, the study develops a similarity index. This index helps distinguish between faulty and healthy phases in the feeders, aiding in fault detection.

The proposed algorithm in this study demonstrates robust performance across various testing scenarios, indicating its effectiveness in real-world applications. Furthermore, the study validates the accuracy of this method through Hardware-in-the-Loop (HIL) testing analysis, showcasing its practical utility.

The proposed method excels in detecting low impedance faults, but it does not address high impedance faults in the microgrid. However, the study acknowledges this limitation and suggests that future works will focus on analyzing and developing methods to detect high impedance faults as well. This acknowledgment points towards ongoing research and development in the field, with potential advancements in fault detection techniques for microgrids.

REFERENCES

[1] V. K. Garg and S. Sharma, "Overview on Microgrid System," 2018 Fifth International Conference on Parallel, Distributed and Grid Computing (PDGC), Solan, India, 2018, pp. 694-699.

[2] Zamani M A, Yazdani A, and Sidhu T S. “A control strategy for enhanced operation of inverter-based microgrids under transient disturbances and network faults,” IEEE Transactions on Power Delivery, vol. 27, no. 4, pp. 1737-1747, Oct. 2012.

[3] Y. Pavankumar, S. Debnath, and S. Paul, “A New Lissajous-Based Technique for Islanding Detection in Microgrid,” IEEE Transactions on Smart Grid, DOI: 10.1109/TSG.2023.3322435.

[4] Sayan Saha, Anushka Debnath, Yadala Pavankumar, et al, “A Lissajous based technique for fault detection and faulty phase identification in transmission line,” 2023 Second International Conference on Electrical, Electronics, Information and Communication Technologies, ICEEICT 2023, 2023.

[5] Nisar A and Thomas M S. “Comprehensive control for microgrid autonomous operation with demand response,” IEEE Transactions on Smart Grid, vol. 8, no. 5, pp. 2081-2089, Sep. 2017.

[6] Dharmapandit O, Patnaik R K, Dash P K. A fast time-frequency response based differential spectral energy protection of AC microgrids including fault location. Protection & Control of Modern Power Systems, 2017, 2(2): 30. DOI 10.1186/s41601-017-0062-0.

[7] Y. Baghzouz, "Voltage regulation and overcurrent protection issues in distribution feeders with distributed generation - a case study", in *Proceedings of the 38th Annual Hawaii International Conference on System Sciences*, Big Island, HI, USA, 2005, pp. 1-7.

[8] J. Driesen, P. Vermeyen, and R. Belmans, "Protection issues in microgrids with multiple distributed generation units", in *Power Conversion Conference (PCC '07)*, Nagoya, Japan, 2007, pp. 646 - 653.

[9] K. L. Butler-Purry and H. B. Funmilayo, "Overcurrent protection issues for radial distribution systems with distributed generators", in *IEEE Power & Energy Society General Meeting*, Calgary, Alberta, Canada, 2009, pp. 1-5.

[10] S. Conti, L. Raffa, and U. Vagliasindi, "Analysis of protection issues in autonomous mv micro-grids", in *20th International Conference on Electricity Distribution*, Prague, Czech Republic, 2009, pp. 1-5.

[11] A. M. Massoud, S. Ahmed, S. J. Finney, and B. W. Williams, "Inverter-based versus synchronous-based distributed generation: fault current limitation and protection issues", in *2010 IEEE Energy Conversion Congress and Exposition (ECCE)*, Atlanta, Georgia, 2010, pp. 58-63.

[12] A. Kazakov, K. Janson, and T. Vaimann, "Microgrids performance challenges", in 11th International Symposium on Topical Problems in the Field of Electrical and Power Engineering and Doctoral School of Energy and Geotechnology II, Pärnu, Estonia, 2012, pp. 42-46.

[13] B. Hussain, S. M. Sharkh, and S. Hussain, "Impact studies of distributed generation on power quality and protection setup of an existing distribution network", in *International Symposium on Power Electronics Electrical Drives Automation and Motion (SPEEDAM)*, Pisa, Italy, 2010, pp. 1243-1246.

[14] T. Gallery, L. Martinez, and D. Klopotan, "Impact of distributed generation on distribution network protection", ESBI Engineering & Facility Management, Ireland.

[15] Nimpitiwan N, Heydt G T, Ayyanar R, and Suryanarayanan S. “Fault current contribution from synchronous machine and inverter based distributed generators,” IEEE Transactions on Power Delivery, vol. 22, no. 1, pp. 634-641, Jan. 2007.

[16] Li X, Dysko A, and Burt G M. “Traveling wave-based protection scheme for inverter-dominated microgrid using mathematical morphology,” IEEE Transactions on Smart Grid, vol. 5, no. 5, pp. 2211-2218, Sep. 2014.

[17] Mirsaeidi S, Said D M, and Mustafa M W. “A protection strategy for micro-grids based on positive-sequence impedance,” IET Renewable Power Generation, vol. 9, no. 6, pp. 600-609, Jan. 2015.

[18] Casagrande E, Woon W L, Zeineldin H H, et al. “A differential sequence component protection scheme for microgrids with inverter-based distributed generators,” IEEE Transactions on Smart Grid, vol. 5, no. 1, pp. 29-37, Jan. 2013.

[19] Che L and Khodayar M E. “Adaptive protection system for microgrids: protection practices of a functional microgrid system,” IEEE Electrification Magazine, vol. 2, no. 1, pp. 66-80, Mar. 2014.

[20] Wai D C T and Xia Y. “A novel technique for high impedance fault identification,” IEEE Transactions on Power Delivery, vol. 13, no. 3, pp. 738-744, Jul. 1998.

[21] Sortomme E, Venkata S S, and Mitra J. “Microgrid protection using communication-assisted digital relays,” IEEE Transactions on Power Delivery, vol. 25, no. 4, pp. 2789-2796, Oct. 2010.

[22] Mirsaeidi S, Said D M, Mustafa M W and Ghaffari K. “Progress and problems in micro-grid protection schemes,” Renewable and Sustainable Energy Reviews, vol. 37, no. 3, pp. 834-839, Sep. 2014.

[23] Gao H and Crossley P A. “Design and evaluation of a directional algorithm for transmission-line protection based on positive sequence fault components,” IEE Proceedings- Generation, Transmission and Distribution, vol. 153, no. 6, pp. 711-718, Nov. 2006.

[24] Pradhan A K, Routray A, and Madhan Gudipalli S, “Fault direction estimation in radial distribution system using phase-change in sequence current,” IEEE Transactions on Power Delivery, vol. 22, no. 4, pp. 2065-2071, Oct. 2007.

[25] Jena P, Pradhan AK. “Directional relaying during single-pole tripping using phase change in negative-sequence current,” IEEE Trans Power Delivery, vol. 28, no. 3, pp. 1548–57, Jul. 2013.

[26] Liu K A and Li Y Y. “Study on solutions for active distribution grid protection,” Proceedings of the CSEE, vol. 34, no. 16, pp. 2584-2590, Jun. 2014.

[27] Zhang F, Mu L, and Guo W. “An integrated wide-area protection scheme for active distribution networks based on fault components principle,” IEEE Transactions on Smart Grid, 2017, PP (99):1-1.

[28] Camacho A, Castilla M, Miret J, and Borrell A. “Active and reactive power strategies with peak current limitation for distributed generation inverters during unbalanced grid faults,” IEEE Transactions on Industrial Electronics, vol. 62, no. 3, pp. 1515-1525, Mar. 2015.

[29] Guo W, Mu L, and Zhang X. “Fault models of inverter-interfaced distributed generators within a low-voltage microgrid,” IEEE Transactions on Power Delivery, vol. 32, no. 1, pp. 453-461, Feb. 2017.

[30] Tafti H D, et al. “Low-voltage ride-thorough capability of photovoltaic grid-connected neutral-point-clamped inverters with active/reactive power injection,” IET Renewable Power Generation, vol. 11, no. 8, pp. 1182-1190, Jan. 2017.

[31] Vrionis T D, Koutiva X I, and Vovos N A. “A genetic algorithm-based low voltage ride-through control strategy for grid connected doubly fed induction wind generators,” IEEE Transactions on Power Systems, vol. 29, no. 3, pp. 1325-1334, May. 2014.

[32] F. Zhang and L. Mu, "A Fault Detection Method of Microgrids With Grid-Connected Inverter Interfaced Distributed Generators Based on the PQ Control Strategy," in IEEE Transactions on Smart Grid, vol. 10, no. 5, pp. 4816-4826, Sept. 2019.

[33] E. Boardman, “The role of integrated distribution management systems in smart grid implementations,” in Proc. IEEE PES GM, Providence, RI, USA, 2010, pp. 1–6.

[34] A. von Meier, E. Stewart, A. McEachern, M. Andersen, and L. Mehrmanesh, “Precision micro-synchro phasors for distribution systems: a summary of applications,” IEEE Trans. Smart Grid, vol. 8, no. 6, pp. 2926–2936, Nov. 2017.

[35] H. Mohsenian-Rad, E. Stewart, and E. Cortez, “Distribution synchro phasors: pairing big data with analytics to create actionable in formation,” IEEE Power Energy Mag., vol. 16, pp. 26–34, May 2018.

[36] O. Ardakanian, Y. Yuan, R. Dobbe, A. von Meier, S. Low, and C. Tomlin, “Event detection and localization in distribution grids with phasor measurement units,” in Proc. IEEE PES GM, Chicago, IL, 2017.

[37] A. Shahsavari, M. Farajollahi, E. M. Stewart, E. Cortez, and H. Mohsenian-Rad, “Situational awareness in distribution grid using micro-PMU data: A machine

learning approach," IEEE Trans. Smart Grid, vol. 10, no. 6, pp. 6167–6177, Nov. 2019.

[38] A. F. Bastos, S. Santoso, W. Freitas, and W. Xu, "Synchro waveform measurement units and applications," in Proc. IEEE PES Gen. Meeting, Atlanta, GA, USA, 2019, pp. 1–5.

[39] M. Izadi and H. Mohsenian-Rad, "Event location identification in distribution networks using waveform measurement units," in Proc. IEEE PES ISGT Europe, The Hague, The Netherlands, 2020, pp. 924–928.

[40] M. Izadi and H. Mohsenian-Rad, "Synchronous waveform measurements to locate transient events and incipient faults in power distribution networks," IEEE Trans. Smart Grid, vol. 12, no. 5, pp. 4295–4307, Sep. 2021.

[41] "SEL-735 power quality and revenue meter." [Online]. Available: https://selinc.com (accessed Jan. 1, 2022).

[42] "iPSR sensor." [Online]. Available: https://www.candura.com (accessed Jan. 1, 2022).

[43] "MM3 overhead line sensor." [Online]. Available: https://www.sentient energy.com (accessed Jan. 1, 2022).

[44] I. Niazazari, H. Livani, A. Ghasemkhani, Y. Liu, and L. Yang, "Event cause analysis in distribution networks using synchro waveform measurements," in Proc. North Amer. Power Symp., Tempe, AZ, USA, 2021, pp. 1–5.

[45] M. Izadi and H. Mohsenian-Rad, "A synchronized Lissajous-based approach to achieve situational awareness using synchronized wave form measurements," in Proc. IEEE PES Gen. Meeting, Washington, DC, USA, 2021, pp. 1–5.

[46] M. Izadi and H. Mohsenian-Rad, "Characterizing synchronized lissajous curves to scrutinize power distribution synchro-waveform measurements," IEEE Trans. Power Syst., vol. 36, no. 5, pp. 4880–4883, Sep. 2021.

[47] M.Izadi and H.Mohsenian-Rad, "Synchronous waveform measurements to locate transient events and incipient faults in power distribution networks," in Proc. IEEE Trans. Smart Grid, May 2021, pp. 1–12.

[48] B. Patel, "A new technique for detection and classification of faults during power swing," Electr. Power Syst. Res., vol. 175, no. June, p. 105920, 2019.

[49] D.Karacor,S.Nazlibilek,M.H.Sazli,andE.S.Akarsu,"Discretelissajous figures and applications," IEEE Trans. Instrum. Meas., vol. 63, no. 12, pp. 2963–2972, Dec. 2014.

[50] A. Abu-Siada and S. Islam, "A novel online technique to detect power transformer winding faults," IEEE Trans. Power Deli., vol. 27, no. 2, pp. 849–857, Apr. 2012.

[51] F. Nejabatkhah and Y. W. Li, "Overview of Power Management Strategies of Hybrid AC/DC Microgrid," IEEE Trans. Power Electron., vol. 30, no. 12, pp. 7072 7089, 2015.

[52] A. Hirsch, Y. Parag, and J. Guerrero, "Microgrids : A review of technologies , key drivers , and outstanding issues," Renew. Sustain. Energy Rev., vol. 90, pp. 402 411, 2018.

[53] F. Katiraei and M. R. Iravani, "Power management strategies for a microgrid with multiple distributed generation units," IEEE Trans. Power Syst., vol. 21, no. 4, pp. 1821–1831, 2006.

[54] G. K. Venayagamoorthy, "Potentials and promises of computational intelligence for smart grids," IEEE Power Energy Soc. Gen. Meet., pp. 1–6, 2009.

[55] N. Eghtedarpour and E. Farjah, "Power control and management in a hybrid AC/DC microgrid," IEEE Trans. Smart Grid, vol. 5, no. 3, pp. 1494–1505, 2014.

[56] S. Monesha, S. G. Kumar, and M. Rivera, "Microgrid Energy Management and Control : Technical Review," IEEE Int. Conf. Autom., pp. 1–7, 2017.

[57] T. Ackermann, G. Andersson, and L. Soder, "Distributed generation : a definition," Electr. Power Syst. Res., vol. 57, pp. 195–204, 2001.

[58] S. Pradhan, D. Mishra, and M. K. Maharana, "Energy Management System for Micro Grid Pertaining to Renewable Energy Sources: A Review," Int. Conf. Innov. Mech. Ind. Appl., pp. 18–23, 2017.

[59] S. I. Gkavanoudis and C. S. Demoulias, "A control strategy for enhancing the Fault Ride-Through capability of a microgrid during balanced and unbalanced grid voltage sags," Sustain. Energy, Grids Networks, vol. 3, pp. 1–11, 2015.

[60] D. Arcos-Aviles, F. Guinjoan, P. M. Marietta, J. Pascual, L. Marroyo, and P. Sanchis, “Energy management strategy for a grid-tied residential microgrid based on fuzzy logic and power forecasting,” IECON 2016 - 42nd Annu. Conf. IEEE Ind. Electron. Soc., pp. 4103–4108, 2016.

[61] A. R. Haron, A. Mohamed, H. Shareef, and H. Zayandehroodi, “Analysis and solutions of overcurrent protection issues in a microgrid,” in 2012 IEEE International Conference on Power and Energy (PECon), Dec 2012, pp. 644–649.

[62] Effect of DG on Distribution Grid Protection. INTECH Open Access Publisher, 2010.

[63] Y. Bansal and R. Sodhi, "Microgrid fault detection methods: Reviews, issues and future trends," 2018 IEEE Innovative Smart Grid Technologies - Asia (ISGT Asia), Singapore, 2018, pp. 401-406.

[64] A. Supannon and P. Jirapong, “Recloser-fuse coordination tool for distributed generation installed capacity enhancement,” in 2015 IEEE ISGT-ASIA, Nov 2015, pp. 1–6.

[65] Guan-Chyun Hsieh, and James C. Hung, "Phase-Locked Loop Techniques-A Survey," iEEE Trans. ind. Electron., vol. 43, no. 6, pp 609-615, Dec. 1996.

[66] Bae Y and Vu T K. “Implemental control strategy for grid stabilization of grid-Connected PV system based on German grid code in symmetrical low-to-medium voltage network,” IEEE Transactions on Energy Conversion, vol. 28, no. 3, pp. 619-631, Sep. 2013.

[67] Yaramasu V, Wu B, Alepuz S, et al. “Predictive control for low-voltage ride-through enhancement of three-level-boost and NPC-converter-based PMSG wind turbine,” IEEE Transactions on Industrial Electronics, vol. 61, no. 12, pp. 6832-6843, Dec. 2014,

[68] Qu L and Qiao W. “Constant power control of DFIG wind turbines with supercapacitor energy storage,” IEEE Transactions on Industry Applications, vol. 47, no. 1, pp. 359-367, Jan/Feb. 2011.

[69] Yang Y, Blaabjerg F and Wang H, "Low-voltage ride-through of single-phase transformerless photovoltaic inverters," IEEE Transactions on Industry Applications, vol. 50, no. 3, pp. 1942-1952, May/Jun. 2014

[70] Dasgupta S, Mohan S N and Sahoo S K, et al. "Lyapunov function-based current controller to control active and reactive power flow from a renewable energy source to a generalized three-phase microgrid system," IEEE Transactions on Industrial Electronics, vol. 60, no. 2, pp. 799-813, Feb. 2012

[71] E. Troester, "New German grid codes for connecting PV systems to the medium voltage power grid," in 2nd International Workshop on Concentrating Photovoltaic Power Plants: Optical Design, Production, Grid Connection, 2009, pp. 1–4.

[72] Timbus A V. "Control strategies for distributed power generation systems operating on faulty grid" in IEEE International Symposium on Industrial Electronics, Montreal, Canada, 2006, pp. 1601-1607.

APPENDIX

Second International Conference on Smart Technologies for Power and Renewable Energy (SPECon)

(Technically Co-Sponsored by IEEE Kerala Section)

IEEE Kerala Section

Best Paper Award

Presented To

Peddinte Siva Durga Satya Prasad

for the paper

"Fault Detection Method for Inverter Interfaced Distributed Generators Based Microgrid" presented on **April 2-4, 2024.**

Dr. Archana R.	Dr. Rabiya Rasheed	Dr. Surya Susan Alex	Ms. Rakhee R	Ms. Soumya Simon
General Chair	Publication Chair	TPC Chair	Publicity Chair	Finance Chair
SPECon	SPECon	SPECon	SPECon	SPECon

Fault Detection Method for Inverter Interfaced Distributed Generators Based Microgrid

Peddinte S D S Prasad
Department of Electrical Engineering
National Institute of Technology
Tadepalligudem, India
siva.peddinte@gmail.com

Yadala Pavankumar
Department of Electrical Engineering
National Institute of Technology
Tadepalligudem, India
pavankumaryadala008@gmail.com

Gubbala S S N S Manikanta
Department of Electrical Engineering
National Institute of Technology
Tadepalligudem, India
gssnsmanikanta@gmail.com

O.Jayasimha Reddy
Department of Electrical Engineering
National Institute of Technology
Tadepalligudem, India
jsreddy0906@gmail.com

***Abstract*— A microgrid is a small power distribution system consisting of a cluster of low-power generation units (micro energy sources) capable of operating independently, loads, energy storage, and energy conversion devices with associated protection and control units. Unlike traditional microgrids, the micro sources in all microgrids are inverter-interfaced distributed generators (IIDGs), in which the fault currents are 1.2-2 times the rated current. To ensure the stable operation of the microgrid requires to detect the faults within the minimum possible time. The data collected from Waveform Measurement Units (WMUs) are widely used to detect disturbances. When an event occurs, WMUs provide GPS-synchronized measurements of voltage and current waveforms in the time domain captured during the event. Given such data, a Lissajous curve can be developed, which is a graph constructed by plotting one waveform versus another. By utilizing this phenomenon, a new algorithm has been developed to detect and locate faults within the microgrid.**

Keywords*— Distributed Generation, Fault detection, Low voltage ride through, Microgrid.

I. INTRODUCTION

A microgrid consists of different electrical loads, energy storage systems (ESS), and distributed generators (DGs). There are two ways that microgrids can function, the first one is grid connected mode in which the microgrid will be integrated to the utility grid and islanded mode of operation where it will work independently. After serving the load demand, it can supply the excess power generation to the utility grid and also it can draw the power from the utility grid whenever it is not able to serve the load [1]. The DGs are interfaced into the grid through power electronic converters makes the control of the real and reactive power injection flexible. When there is a fault within the microgrid, the DGs should have low voltage ride through (LVRT) or fault ride through (FRT) or under voltage ride through (UVRT) for predetermined amounts of time in milliseconds to support the voltage at the PCC in accordance with utility standards. Under these circumstances, they continue to be integrated to the grid and provide the reactive power for a specified time [2]. Most of the micro sources in the microgrid are inverter-interfaced distributed generators (IIDGs), and the fault characteristics of IIDGs differ from those of conventional synchronous generators. The maximum output fault current of the IIDG is typically limited to 1.2-2 times the rated current [3].

The traditional fault detection methods are schemes based on the overcurrent principle, distance-based relay systems, and methods based on current harmonic distortions [4-6]. When the renewable-based DGs are integrated into the microgrid, the power flow becomes bidirectional, hence these are not applicable in the microgrid since majority of these schemes are designed for unidirectional power flow systems [7]. Using IIDG-based microgrids, these characteristics create significant challenges for fault detection. It is necessary to discover an appropriate fault detection technique for microgrids in order to support the practical implementation of these systems. In the past few years, researchers have studied microgrid fault detection techniques extensively.

Ref. [8] suggested a fault components principle-based integrated wide-area protection method. By analysing the phase difference between the positive-sequence current fault components and the main feeder and slave feeders in various area protection units, a fault location was identified. Furthermore, the conventional fault components additional network analysis approach was applied. But the IIDGs specific control strategy has not been taken into the account, as a result, they are only comparable to a steady power or current source. Ref. [9] introduced a fault detection technique utilising the phase shift in the negative-sequence current. It was suggested to use the phase change in the negative-sequence current as a directional relaying technique during single-pole tripping. The algorithm, however, does not identify a fault with the branch feeder and is unable to find the problematic phase. In Ref. [10] a new fault detection scheme has been introduced for the microgrid based on the phase change in the positive sequence feeder current. The DGs are working under LVRT and the proposed method has different approaches for different operating conditions of the DGs. An optimization based local fault detector is designed in [11] for distributed generator based microgrid which depends on the local measured state of the subsystem as well as the neighbouring measurements of the transmitted variables.

Waveform measurement units (WMUs) have been used as smart sensors in recent years. The WMUs has a high reporting rate and can offer accurate information on time-synchronized waveform measurements of voltage and current. These WMUs can be utilized to observe the voltage and current waveform under disturbances such as faults, capacitor switching's, islanding of the loads and DGs etc., which has to be identified in less time for safe and continuous operation of the microgrid. The voltage and current waveforms can be used to generate the Lissajous figure [12,13]. The Lissajous figure can be utilized to pinpoint the

origin of systemic events due to its distinct behavior under various conditions. Consequently, the authors of this study aim to leverage the properties of the Lissajous figure to introduce a new fault detection method for microgrids.

Based on the properties of the Lissajous figure at each feeder, this study proposes a novel method for low impedance fault detection in the microgrid consists of IIDGs (which are having LVRT capability). The summary of the primary contributions made by this study are:

1) It is observed that the Lissajous curve shape changes under different conditions. During normal conditions, the Lissajous curve is elliptic; however, when a fault arises, its shape changes. Therefore, on the basis of this phenomenon a novel method for microgrid fault detection is developed.

2) The change in the Lissajous curve results the change in the area of the curve. Hence two successive areas are monitored to develop the fault index in the proposed approach. Once a fault occurs, the area changes, indicating that fault has occurred and the similarity index values can identify the start time of fault event.

3) The proposed algorithm has considered the thresholds to distinguish between the faulty phase and healthy phase of the feeders.

II. The Microgrid Test System

A basic model of a microgrid, as depicted in Fig. 1, is constructed following the IEEE 1547 standard and the overview provided by the Consortium for Electric Reliability Technology Solutions (CERTS). The microgrid model operates in grid-connected mode in which the IIDGs operates in current control mode (PQ-control), where it utilizes the grids voltage and current as reference at the PCC. The test system consists of three loads denoted as LOAD1-LOAD3 and the distributed generators are referred to as DG1 and DG2. The circuit breakers (CBs) for the feeders are labeled as A1-A4, B1-B3, and C1-C3. The Main feeders, such as L3 and L4, have CBs at both the ends while branch feeders, such as L1, L2, L5, L6, L7, and L8, have CBs placed at upstream.

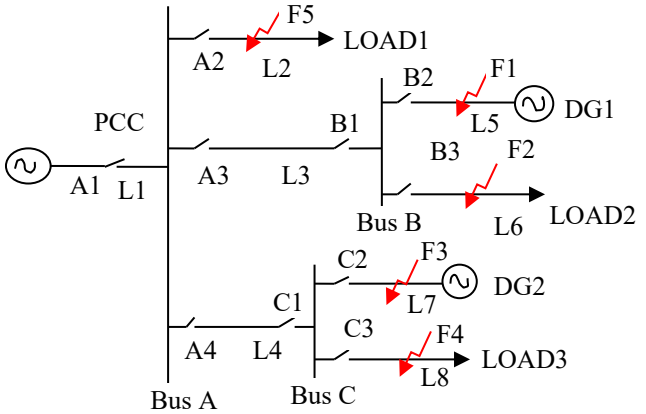

Fig. 1. Basic Microgrid Test System.

The microgrid test system comprises two wind-based IIDGs rated at 500 kW and 600 kW, respectively. Each is connected to a main feeder through circuit breakers. The lengths of the feeders are as follows: L1 = 5 km, L2 = 15 km, L3 = 5 km, L4 = 8 km, L5 = 12 km, L6 = 12 km, L7 = 12 km, and L8 = 12 km. L2, L6, and L8 are connected to series RLC loads, while L5 and L7 are connected to IIDGs, and main feeders L3 and L4. Load 1 consists of R1 = 1.4 Ω, L1 = 95.6 H, and C1 = 3.184 μF; load 2 comprises R2 = 1.3 Ω, L2 = 636.95 H, and C2 = 3.184 μF; load 3 includes R3 = 1.4 Ω, L3 = 1019.11 H, and C3 = 3.184 μF. The system operates at a grid frequency of 50 Hz with an operating voltage of 10 kV. The IIDGs supports the LVRT capability, whenever fault occurs for every 1% voltage drop IIDG suplies 2% reactive current when the voltage level is between 90% to 50% and if the voltage level is below 50% it will inject maximum reactive power.

III. Fault Detection Using Lissajous Figures

A Lissajous curve is a graphic representation of the voltage and current signals that were obtained from each feeder.

A. Illustration of the Lissajous Figure

The signals for the instantaneous voltage and current are expressed as

$$v = V_o \sin(wt) \tag{1}$$

$$i = I_o \sin(wt + \delta) \tag{2}$$

where V_o and I_o are the voltage and current signal amplitudes, respectively, and δ is the power factor angle. The voltage signal is placed in the y-axis and the current signal is placed in the x-axis to create the Lissajous figure. Next, we obtain the relationship between waveform v and waveform i by eliminating wt from equations (1) and (2). Accordingly, from (1), we have:

$$wt = \sin^{-1}\left(\frac{v}{V_o}\right) \tag{3}$$

By substituting (3) in (2) we can obtain as follows:

$$i = I_o \sin\left(\sin^{-1}\left(\frac{v}{V_o}\right) + \delta\right) \tag{4}$$

By applying the trigonometric identities to solve (4), (5) can be obtained.

$$\frac{i}{I_o} - \frac{v}{V_o}\cos\delta = \sin\delta\sqrt{1 - \left(\frac{v}{V_o}\right)^2} \tag{5}$$

Squaring on both sides to (5), we can obtain (6)

$$\frac{i^2}{I_o^2} - 2\frac{\cos\delta}{I_o V_o} iv + \frac{v^2}{V_o^2} - sin^2\delta = 0 \tag{6}$$

The general equation of 2^{nd} degree is (7)

$$Ax^2 + 2Hxy + By^2 + 2Gx + 2Fy + C = 0 \tag{7}$$

By comparing (6) and (7) we get the values of

$$A = {}^1/_{I_o^2}, \quad H = -\frac{\cos\delta}{I_o V_o}, \quad B = {}^1/_{V_o^2}, \quad G = 0, \quad F = 0, \quad C = -sin^2\delta \tag{8}$$

So, equation (6) always represents an ellipse because

$$H^2 - AB < 0 \tag{9}$$

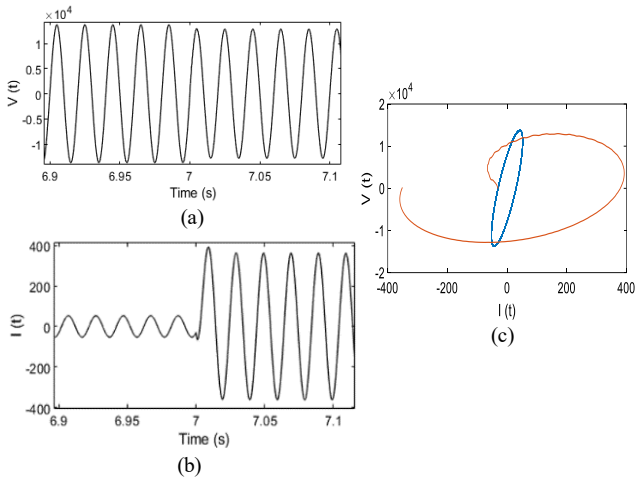

Fig. 2. (a) Voltage signal (b) Current signal (c) Lissajous figure of corresponding voltage and Current signal.

Hence, in Fig. 2 under normal operating conditions, the Lissajous curve that is produced based on the v vs i is always an ellipse. The Lissajous figure deviates from its original elliptical shape (blue colour) when fault occurs because it disrupts the voltage and current signals at the respective feeder. As a result, under a fault event, the Lissajous figure shape changes (orange colour).

B. *Fault Detection method*

The fault detection technique is developed based on the data from WMUs and the associated Lissajous curve. The suggested technique is predicated on changes in the Lissajous curve area during two consecutive cycles.

Let's define the area of the Lissajous curve at time 't' over period T as follows:

$$Area_{v-i}(t) = \left|\int_{i(\tau=t-T)}^{i(\tau=t)} v(\tau)di(\tau)\right| \quad (10)$$

At normal condition the successive areas are almost equal. For instance, at normal operating condition, if $Area_{v-i}(t)$ is the area at time 't' and $Area_{v-i}(t-\Delta t)$ is the area at time 't-Δt', both will be almost equal, where 'Δt' is the time interval. There will be some variation between the $Area_{v-i}(t)$ and $Area_{v-i}(t-\Delta t)$ if any event happens at time 't'. Thus, in order to identify the fault condition, a similarity index based on the area of the Lissajous figure as illustrated in (11) has been developed.

$$SI(t) = 1 - \left|\frac{Area_{v-i}(t) - Area_{v-i}(t-\Delta t)}{max\{Area_{v-i}(t), Area_{v-i}(t-\Delta t)\}}\right| \quad (11)$$

SI(t) is near to one if the areas of the two consecutive Lissajous curves are almost equal. SI(t) comes near to zero when the areas of the two succeeding Lissajous curves differ significantly which indicates that there has been an abrupt change in the Lissajous curve at time 't'. This indicates that fault occurred at time 't'.

C. *Proposed Algorithm*

When a fault occurs, the entire microgrid system will be disturbed. Therefore, it is necessary to calculate the Similarity Index (SI) at every Circuit Breaker (CB). By calculating the SI at the CBs and comparing with the threshold we can differentiate between faulty phase and healthy phase and also the fault locations. In the proposed algorithm, two thresholds, T1 and T2, have been considered. T1 is the threshold given to the main feeders and DG feeders while T2 is used for load feeders. By analyzing the SI for all faults at every CB of the microgrid test system as shown in Fig. 1, the thresholds have been selected as 0.17 and 0.26 respectively for T1 and T2.

The branch feeders L5, L6, L7 and L8 are connected to the main feeders L3 and L4 therefore any disturbance occurs in the branch feeders will affect the main feeders. Hence the

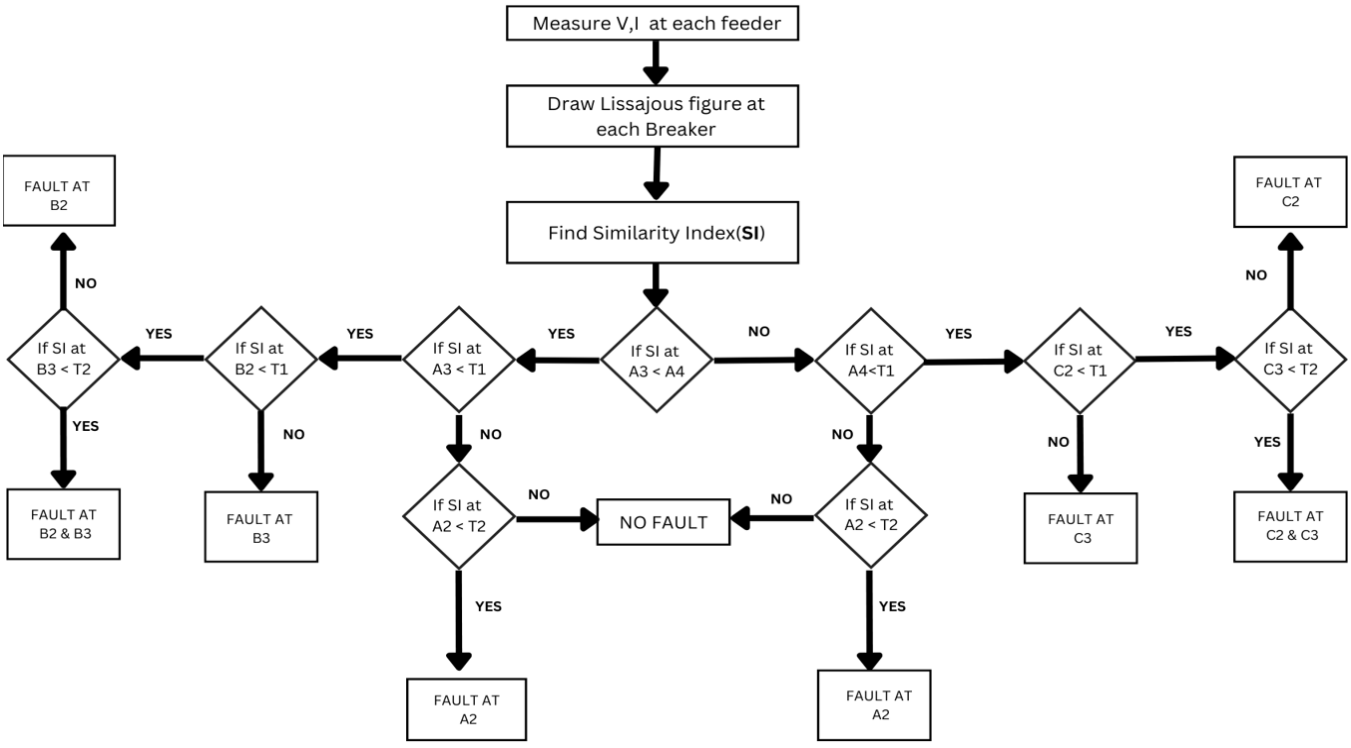

Fig. 3. Flowchart of proposed algorithm.

proposed fault detection scheme is initiated by checking the SI at the main feeders as shown in the Fig. 3 and explained below.

Case 1: If SI at CB-A3 is less than CB-A4, then check if the SI of CB-A3 is less than T1. If it is less than T1, then the fault is at CB-B2 or CB-B3 (because the feeders L5 and L6 are connected to the main feeder L3). If the SI of CB-B2 is less than T1, then fault is occurred at that CB-B2 or If the SI of CB-B3 is less than T2, then fault is occurred at that CB-B3. If it is not less than T1 and if the SI of CB-A2 is less than T1, then fault is occurred at CB-A2.

Case 2: If SI at CB-A3 is greater than CB-A4, then check if the SI of CB-A4 is less than T1. If it is less than T1, then the fault is at CB-C2 or CB-C3; otherwise, the fault is at CB-A2 (if it is less than T2). If the SI of CB-C2 is less than T1, then fault is occurred at that CB-C2. If the SI of CB-C3 is less than T2, then fault is occurred at that CB-C3.

The proposed method only utilizes the voltage and current signals at each breaker (preferably in p.u) and analyses the waveform behavior and detects the faults hence the size of the DGs doesn't affect the proposed scheme and also it doesn't add any additional disturbance signals into the system. Therefore, it will not lead to power quality issues.

IV. Results

The proposed fault detection method has been validated for the test system shown in Fig. 1 in the MATLAB\Simulink environment. The fault leads the feeder currents and voltages to disturbance, therefore the variations in phase and magnitude of three phases of the feeders has been observed. In this study different asymmetrical and symmetrical faults are considered such as LG, LL, LLG, LLL and LLLG.

A. Line to Ground Fault (LG)

A single line to ground fault typically happens when one conductor touches the neutral conductor or falls to the ground. In our study, the LG fault is characterized by a Fault resistance (R_{on}) = 0.1 Ω and Ground resistance (R_g) = 0.01 Ω. The switching times are set between 7 to 10 secs. The LG fault is applied to L5 feeder, which is having DG1. The obtained SI values at different CBs are given in Fig. 4. When a fault occurs in a branch feeder, the main feeder associated with the same branch feeder is more affected by the fault compared to other main feeders. In this case, as it is a LG fault at L5, the SI for a single phase at CB-A3 and CB-B2 only becomes less the threshold, as observed in Fig. 4 (b) and 4(d), which is not true at any other CB therefore the proposed method detects the fault at CB-B2 which is true. The obtained results for LG fault at other locations given in Table I, which displays the similarity index (SI) of all circuit breakers (CBs) when a LG fault occurs, affecting only a single phase.

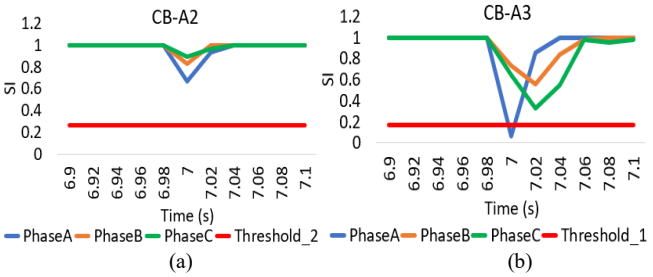

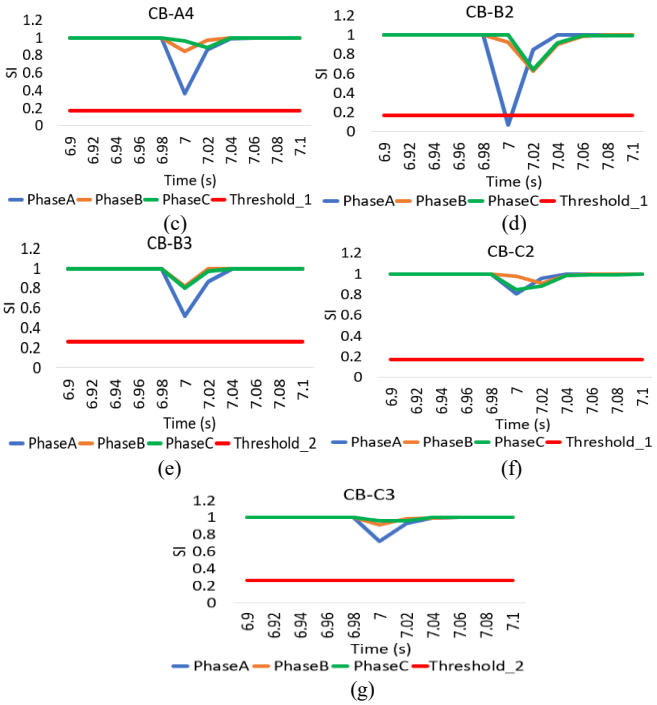

Fig. 4. When LG Fault occurs on CB-B2 at 7 secs: (a) SI values at CB-A2, (b) SI values at CB-A3, (c) SI values at CB-A4, (d) SI values at CB-B2, (e) SI values at CB-B3, (f) SI values at CB-C2, (g) SI values at CB-C3.

B. Line to Line Fault (LL)

A LL fault occurs when two lines are short-circuited. The LL fault is characterized by a Fault resistance (R_{on}) = 0.1 Ω, and switching times between 7 to 10 secs. In Fig. 5, The SI values at CB-A3 and CB-B2 are given when a LL fault occurs at L5. The Results shows that the SI for two phases becomes less than the threshold since it is a LL fault, while the remaining feeders are not significantly affected. Table II indicates the results for LL fault at different locations, and the results shows that the proposed method can identify the faults accurately. Table II will also shows the SI of all CBs when a LL fault occurs, affecting two phases of the feeders.

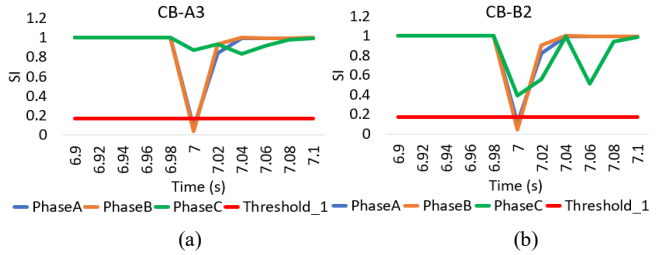

Fig. 5. When LL Fault occurs on CB-B2 at 7 secs: (a) SI values at CB-A3, (b) SI values at CB-B2.

C. Double Line to Line Ground (LLG)

A LLG fault occurs when two lines come in contact with each other along with the ground. The LLG fault considered at L6 which is characterized by a Fault resistance (R_{on}) = 0.1 Ω, Ground resistance (R_g) = 0.01 Ω, and switching times between 7 to 10 secs. The Obtained SI values at CB-A3 and CB-B3 has been depicted in Fig. 6. Since it is a LLG fault, resulting the SI value for two phases has become less than the thresholds (SI at CB-A3<T1 and SI at CB-B3<T2), while the remaining feeders are not significantly affected. The LLG faults are considered at different locations and the results are given in Table III, which presents the SI of all CBs when a

TABLE I. SI OF ALL CBS WHEN LG FAULT OCCURS AT 7SECS

Fault Location	SI at CB-A2			SI at CB-A3			SI at CB-A4			SI at CB-B2			SI at CB-B3			SI at CB-C2			SI at CB-C3		
	Phases			*Phases*			*Phases*			*Phases*			*Phases*			*Phases*			*Phases*		
	A	*B*	*C*	*A*	*B*	*C*	*A*	*B*	*C*	*A*	*B*	*C*	*A*	*B*	*C*	*A*	*B*	*C*	*A*	*B*	*C*
CB-A2	**0.10**	0.63	0.70	0.32	0.81	0.95	0.43	0.87	0.95	0.82	0.94	0.86	0.74	0.91	0.95	0.81	0.95	0.86	0.76	0.94	0.97
CB-B2	0.66	0.82	0.89	**0.06**	0.73	0.64	0.36	0.84	0.96	**0.07**	0.92	0.99	0.52	0.81	0.79	0.80	0.97	0.84	0.72	0.91	0.96
CB-B3	0.67	0.85	0.90	**0.06**	0.52	0.77	0.37	0.86	0.96	0.83	0.91	0.70	**0.12**	0.70	0.70	0.79	0.96	0.85	0.73	0.92	0.95
CB-C2	0.73	0.85	0.92	0.40	0.82	0.97	**0.11**	0.83	0.72	0.86	0.98	0.88	0.76	0.90	0.95	**0.09**	0.87	0.99	0.54	0.85	0.82
CB-C3	0.71	0.86	0.91	0.33	0.82	0.97	**0.10**	0.61	0.86	0.83	0.96	0.86	0.74	0.91	0.95	0.60	0.93	0.65	**0.16**	0.74	0.72

TABLE II. SI OF ALL CBS WHEN LL FAULT OCCURS AT 7SECS

Fault Location	SI at CB-A2			SI at CB-A3			SI at CB-A4			SI at CB-B2			SI at CB-B3			SI at CB-C2			SI at CB-C3		
	Phases			*Phases*			*Phases*			*Phases*			*Phases*			*Phases*			*Phases*		
	A	*B*	*C*	*A*	*B*	*C*	*A*	*B*	*C*	*A*	*B*	*C*	*A*	*B*	*C*	*A*	*B*	*C*	*A*	*B*	*C*
CB-A2	**0.11**	**0.06**	0.84	0.42	0.34	0.86	0.49	0.42	0.88	0.86	0.74	0.59	0.77	0.82	0.88	0.85	0.71	0.57	0.77	0.83	0.90
CB-B2	0.75	0.78	0.81	**0.07**	**0.03**	0.87	0.40	0.22	0.86	**0.11**	**0.04**	0.38	0.46	0.58	0.72	0.84	0.63	0.50	0.72	0.79	0.88
CB-B3	0.77	0.79	0.82	**0.07**	**0.04**	0.87	0.43	0.31	0.87	0.70	0.48	0.33	**0.17**	**0.08**	0.73	0.85	0.66	0.52	0.73	0.80	0.88
CB-C2	0.81	0.83	0.85	0.53	0.33	0.86	**0.12**	**0.06**	0.86	0.93	0.73	0.62	0.79	0.83	0.90	**0.16**	**0.05**	0.18	0.45	0.58	0.76
CB-C3	0.80	0.82	0.84	0.47	0.32	0.86	**0.11**	**0.06**	0.87	0.90	0.73	0.60	0.78	0.82	0.88	0.68	0.41	0.19	**0.25**	**0.11**	0.73

TABLE III. SI OF ALL CBS WHEN LLG FAULT OCCURS AT 7SECS

Fault Location	SI at CB-A2			SI at CB-A3			SI at CB-A4			SI at CB-B2			SI at CB-B3			SI at CB-C2			SI at CB-C3		
	Phases			*Phases*			*Phases*			*Phases*			*Phases*			*Phases*			*Phases*		
	A	*B*	*C*	*A*	*B*	*C*	*A*	*B*	*C*	*A*	*B*	*C*	*A*	*B*	*C*	*A*	*B*	*C*	*A*	*B*	*C*
CB-A2	**0.09**	**0.06**	0.92	0.27	0.22	0.79	0.39	0.31	0.83	0.88	0.76	0.66	0.69	0.75	0.97	0.87	0.73	0.65	0.70	0.74	0.97
CB-B2	0.59	0.74	0.95	**0.06**	**0.03**	0.94	0.27	0.11	0.81	**0.08**	**0.03**	0.73	0.32	0.50	0.83	0.85	0.64	0.61	0.64	0.71	0.97
CB-B3	0.61	0.74	0.96	**0.06**	**0.03**	0.74	0.31	0.19	0.83	0.72	0.51	0.57	**0.14**	**0.07**	0.89	0.85	0.68	0.64	0.67	0.72	0.96
CB-C2	0.68	0.80	0.97	0.38	0.29	0.80	**0.10**	**0.06**	0.94	0.95	0.76	0.69	0.70	0.78	0.98	**0.12**	**0.05**	0.71	0.34	0.49	0.85
CB-C3	0.66	0.77	0.97	0.31	0.23	0.80	**0.09**	**0.06**	0.79	0.91	0.75	0.68	0.69	0.75	0.97	0.70	0.44	0.52	**0.21**	**0.10**	0.87

TABLE IV. SI OF ALL CBS WHEN LLLG OR LLL FAULT OCCURS AT 7SECS

Fault Location	SI at CB-A2			SI at CB-A3			SI at CB-A4			SI at CB-B2			SI at CB-B3			SI at CB-C2			SI at CB-C3		
	Phases			*Phases*			*Phases*			*Phases*			*Phases*			*Phases*			*Phases*		
	A	*B*	*C*	*A*	*B*	*C*	*A*	*B*	*C*	*A*	*B*	*C*	*A*	*B*	*C*	*A*	*B*	*C*	*A*	*B*	*C*
CB-A2	**0.08**	**0.06**	**0.07**	0.33	0.18	0.28	0.42	0.24	0.36	0.94	0.81	0.81	0.68	0.67	0.73	0.93	0.78	0.79	0.69	0.67	0.72
CB-B2	0.60	0.63	0.68	**0.04**	**0.04**	**0.04**	0.27	0.07	0.23	**0.06**	**0.05**	**0.06**	0.32	0.28	0.39	0.87	0.71	0.72	0.63	0.59	0.65
CB-B3	0.63	0.65	0.70	**0.05**	**0.04**	**0.05**	0.33	0.13	0.27	0.83	0.69	0.66	**0.12**	**0.10**	**0.12**	0.89	0.73	0.74	0.65	0.63	0.68
CB-C2	0.69	0.71	0.75	0.41	0.19	0.29	**0.08**	**0.06**	**0.08**	0.97	0.81	0.82	0.70	0.66	0.69	**0.09**	**0.07**	**0.09**	0.33	0.27	0.39
CB-C3	0.67	0.69	0.74	0.35	0.16	0.27	**0.07**	**0.06**	**0.07**	0.95	0.80	0.79	0.69	0.66	0.69	0.80	0.60	0.57	**0.18**	**0.15**	**0.18**

LLG fault occurs, affecting two phases of the feeders.

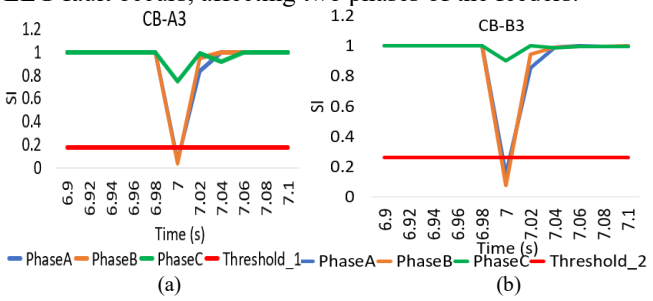

Fig. 6. When LLG Fault occurs on CB-B3 at 7 secs: (a) SI values at CB-A3, (b) SI values at CB-B3.

D. Line to Line to Line Fault (LLL) and Line to Line to Line Ground Fault (LLLG)

These are symmetrical faults. Both faults are characterized by a Fault resistance (R_{on}) = 0.1 Ω, and switching times between 7 to 10 secs. Additionally, for LLLG fault Ground resistance (R_g) = 0.01 Ω is also considered. In Fig. 7, the SI values when LLL occurs at L5 are given. In this case, the SI for all the three phases have become less than the threshold, while the remaining feeders are not significantly affected. Therefore, the proposed method identifies this as a LLL fault. It is observed that LLLG fault also gives the same results. Table IV gives the information of LLL and LLLG faults at different locations, providing the SI of all CBs when LLLG or LLL fault occurs, affecting all the three phases of the feeders.

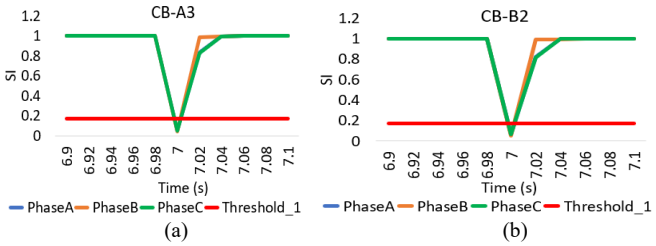

Fig. 7. When LLL Fault occurs on CB-B2 at 7 secs: (a) SI values at CB-A3, (b) SI values at CB-B2.

E. Hardware- in-the-Loop Testing

Through the use of a real-time simulator and an HIL simulation, comparable hardware dynamics are created; indirectly, this results in the creation of a virtual plant that replicates genuine hardware. As a result, the suggested approach has been verified for real-time applications through

HIL testing. The four components of the HIL testing setup taken into consideration in this study are as follows:1) Real Time Digital Simulator (RTDS), an industrial standard HIL testing apparatus that simulates the proposed system in real time; 2) RT Lab software, which is used to run the simulation in real time digital simulator. 3) Computer unit, which operates the RT lab, maintains the measurement data, and runs the algorithm; 4) Multi channel digital oscilloscope, which serves as the external waveform measurement unit (WMU) hardware to store and record the waveform data. To verify the feasibility of the proposed technique in real-time applications, the test model presented in Fig. 1 has been simulated in RTDS using the RT lab software, when LG fault occurs at CB-A2.

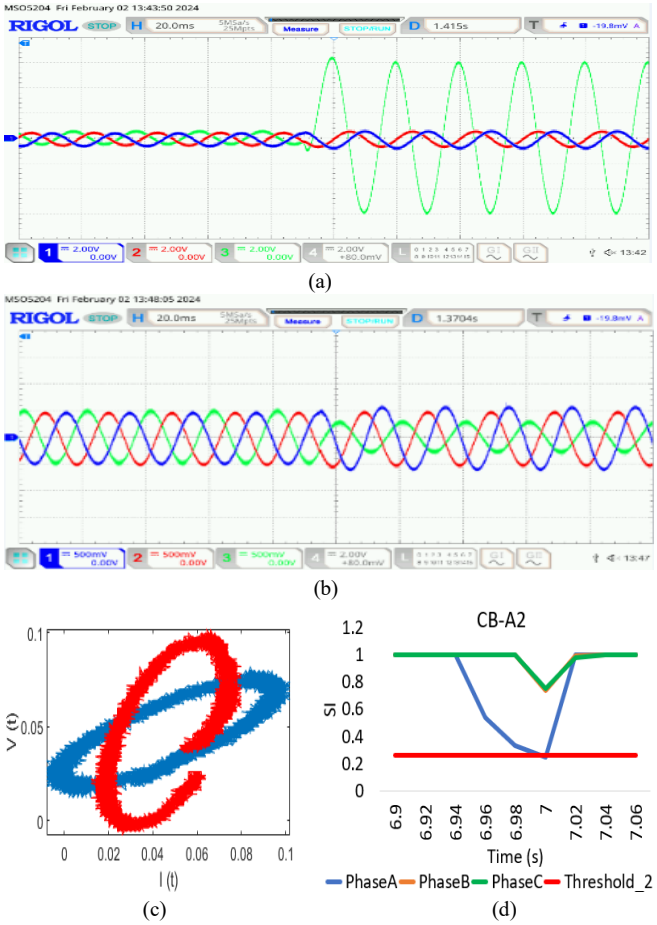

Fig. 8. HIL testing results of fault detection at CB-A2: (a) Current signal, (b) Voltage signal (c) Lissajous figure of corresponding voltage and Current signal. (d) SI values at CB-A2.

To draw the Lissajous figure and to calculate the similarity index, the voltage and current signals are obtained from the digital oscilloscope at each circuit breaker. In Fig. 8 (a) and (b), the current and voltage signals are shown before and after the occurrence of the LG fault, while in Fig. 8 (c) and (d), the corresponding Lissajous figure and SI at CB-A2 are shown. From the results it can be seen that SI for One phase is becomes below the threshold value at CB-A2 which is not observed elsewhere hence the proposed method detects it as a fault at feeder L2 which is true.

The proposed method is able to detect all kinds of the faults in very less time (0.02s) which allows the microgrid system to isolate the faulty section from the system in less time. Hence the operation of the DGs will not be affected severely therefore the stability of the system will be more.

V. Conclusion

This study offers a novel technique to detect low impedance fault in the microgrid by using the Lissajous figure patterns. A similarity index has been developed based on the characteristics of the Lissajous figure at each circuit breaker to identify and distinguish faulty phase and healthy phase of the feeders. The proposed algorithm performs satisfactorily when tested under a variety of circumstances. Additionally, the HIL testing analysis demonstrates the high accuracy of the suggested method for practical applications. However, the proposed method has not considered the high impedance faults, which will be analyzed in the future works.

Acknowledgment

The authors would like to thank the CRTDH project managers of NIT-AP for providing OPAL-RT facilities.

References

[1] V. K. Garg and S. Sharma, "Overview on Microgrid System," 2018 Fifth International Conference on Parallel, Distributed and Grid Computing (PDGC), Solan, India, 2018, pp. 694-699.

[2] S. I. Gkavanoudis and C. S. Demoulias, "A control strategy for enhancing the Fault Ride-Through capability of a microgrid during balanced and unbalanced grid voltage sags," Sustain. Energy, Grids Networks, vol. 3, pp. 1–11, 2015.

[3] Y. Pavankumar, S. Debnath and S. Paul, "Microgrid fault detection technique using phase change of positive sequence current," *International Journal of Modelling and Simulation*, Volume 43, Issue 3, pp. 171-184, 2023.

[4] Mahat P, Chen Z, Bak-Jensen B, et al. A simple adaptive overcurrent protection of distribution systems with distributed generation. IEEE Trans Smart Grid. 2011;2 (3):428–437.

[5] Chilvers I, Jenkins N, Crossley P. Distance relaying of 11 kV circuits to increase the installed capacity of distributed generation. IEE Proc - Gener Transm Distrib. 2005;152(1):40.

[6] Petit M, Le Pivert X, Garcia-Santander L. Directional relays without voltage sensors for distribution networks with distributed generation: use of symmetrical components. Electr Power Syst Res. 2010;80 (10):1222–1228.

[7] Sharma NK, Samantaray SR. Assessment of PMU-based wide-area angle criterion for fault detection in microgrid. IET Gener Transm Distrib. 2019;13(19):4301–4310.

[8] Zhang F, Mu L, and Guo W. "An integrated wide-area protection scheme for active distribution networks based on fault components principle," IEEE Transactions on Smart Grid, 2017, PP (99):1-1.

[9] Jena P, Pradhan AK. "Directional relaying during single-pole tripping using phase change in negative-sequence current," IEEE Trans Power Delivery, vol. 28, no. 3, pp. 1548–57, Jul. 2013.

[10] F. Zhang and L. Mu,. A Fault Detection Method of Microgrids with Grid-Connected Inverter Interfaced Distributed Generators Based on the PQ Control Strategy. *IEEE Trans. Smart Grid*, Sep. 2018.

[11] M. Mola, A. Afshar, N. Meskin and M. Karrari, "Distributed Fast Fault Detection in DC Microgrids," in *IEEE Systems Journal*, vol. 16, no. 1, pp. 440-451, March 2022, doi: 10.1109/JSYST.2020.3035323.

[12] Y. Pavankumar, S. Debnath, and S. Paul, "A New Lissajous-Based Technique for Islanding Detection in Microgrid," *IEEE Transactions on Smart Grid,* DOI: 10.1109/TSG.2023.3322435.

[13] Sayan Saha, Anushka Debnath, Yadala Pavankumar, et al, "A Lissajous based technique for fault detection and faulty phase identification in transmission line," 2023 Second International Conference on Electrical, Electronics, Information and Communication Technologies, ICEEICT 2023, 2023.